INTERNATIONAL JOURNAL OF CLIMATOLOGY
Int. J. Climatol. (2011)
Published online in Wiley Online Library
(wileyonlinelibrary.com) DOI: 10.1002/joc.3396

RMetS
Royal Meteorological Society

Climate change projections for Switzerland based on a Bayesian multi-model approach

A. M. Fischer,[a]* A. P. Weigel,[a] C. M. Buser,[c] R. Knutti,[b] H. R. Künsch,[c] M. A. Liniger,[a] C. Schär[b] and C. Appenzeller[a]

[a] *Federal Office of Meteorology and Climatology, MeteoSwiss, Zurich, Switzerland*
[b] *Institute for Atmospheric and Climate Science, ETH Zurich, Switzerland*
[c] *Seminar for Statistics, ETH Zurich, Switzerland*

ABSTRACT: Regional projections of future climate with associated uncertainty estimates are increasingly being demanded. Generally, such scenarios rely on a finite number of model projections and are accompanied by considerable uncertainties which cannot be fully quantified. Consequently, probabilistic climate projections are conditioned on several subjective assumptions which can be treated in a Bayesian framework. In this study, a recently developed Bayesian multi-model combination algorithm is applied to regional climate model simulations from the ENSEMBLES project to generate probabilistic projections for Switzerland. The seasonal temperature and precipitation scenarios are calculated relative to 1980–2009 for three 30-year scenario periods (centred at 2035, 2060, and 2085), three regions, and the A1B emission scenario. Projections for two further emission scenarios are obtained by pattern scaling. Key to the Bayesian algorithm is the determination of prior distributions about climatic parameters. It is shown that the prior choice of model projection uncertainty ultimately determines the uncertainty in the climate change signal. Here, we assume that model uncertainty is fully sampled by the climate models available. We have extended the algorithm such that internal decadal variability is also included in all scenario calculations. The A1B scenarios show a significant rise in temperature increasing from 0.9–1.4 °C by 2035 (depending upon region and season), to 2.0–2.9 °C by 2060, and to 2.7–4.1 °C by 2085. Mean precipitation changes are subject to large uncertainties with median changes close to zero. Significant signals are seen towards the end of the century with a summer drying of 18–24% depending on region, and a likely increase of winter precipitation in Switzerland south of the Alps. The A2 scenario implies a warming of 3.2–4.8 °C, and a summer drying of 21–28% by 2085, while in case of the mitigation scenario RCP3PD, climate change could be stabilized to 1.2–1.8 °C of warming and 8–10% of drying. Copyright © 2011 Royal Meteorological Society

KEY WORDS regional climate change projections of temperature and precipitation; Bayesian multi-model combination; internal decadal variability; model uncertainty from RCM and GCM; pattern scaling; model bias assumption; Switzerland; ENSEMBLES

Received 26 April 2011; Revised 3 August 2011; Accepted 9 October 2011

1. Introduction

Given the changes in the climate system that have been observed worldwide during the past decades (IPCC, 2007), the demand for reliable and quantitative projections of future climate is continuously growing. The magnitude and severity of climatic changes are thereby expected to be spatially heterogeneous, and the induced impacts upon society, economy, and ecosystems may differ from region to region. For instance, it has been shown that warming trends over western Europe are much stronger than expected from climate model projections (van Oldenborgh, *et al*., 2009), and there are indications that in particular, coastal, high-latitudinal, and mountainous regions belong to the most affected and vulnerable areas (IPCC, 2007). Switzerland, for example, has experienced positive temperature trends over the past 30 years that were around 1.6 times larger than the mean warming trend of the Northern Hemisphere (Ceppi, *et al*., 2010). This underlines the importance for accurate climate change information on regional to local scales, i.e. scales that are most relevant for end users and decision makers for effective climate adaptation and risk management. Much of our knowledge about possible future changes in the climate over Central Europe and Switzerland is based on the analysis of high-resolution regional climate model (RCM) projections. Within the European projects EU FP5 PRUDENCE (Christensen and Christensen, 2007; Jacob, *et al*., 2007) and EU FP6 ENSEMBLES (van der Linden and Mitchell, 2009), such simulations were run in a coordinated multi-institutional effort, bundling the expertise of multiple modelling centres. The conclusions of both projects agree in that they project for all of Europe, by the end of this century, an increase of temperature by several degrees, and for

* Correspondence to: A. M. Fischer, Climate Services, Federal Office of Meteorology and Climatology (MeteoSwiss), Krähbühlstrasse 58, 8044 Zürich, Switzerland. E-mail: andreas.fischer@meteoswiss.ch

the Mediterranean as well as parts of Central Europe a decrease in summer precipitation (Rowell and Jones, 2006; Christensen and Christensen, 2007). Along with changes in the mean, several studies further find an increase in variability of summer temperatures on inter-annual to daily time scales, accompanied by an increase in the frequency of heatwaves (e.g. Schär *et al*., 2004; Scherrer *et al*., 2005; Vidale *et al*., 2007; Fischer and Schär, 2009; Fischer and Schär, 2010) that can at least partly be explained by land–atmosphere feedback processes (Seneviratne *et al*., 2006; Fischer *et al*., 2007).

Several countries have started to disseminate national climate change scenarios on a regular basis (e.g. Lenderink *et al*., 2007; Jenkins *et al*., 2009; Klein Tank and Lenderink, 2009). On the basis of state-of-the-art climate model simulations carried out in the context of the ENSEMBLES project, a report on expected changes in physical climate in Switzerland has been published (CH2011, 2011). It is the aim of this study to describe some of the methodological background of this report. As will become evident with what follows, the route from raw model output to reliable projections of climate change is not trivial but involves a range of assumptions and methodological challenges, some of them being of rather fundamental nature. Here, we discuss these assumptions and challenges, and we propose options of how they can be accounted for. While the methodology proposed is illustrated in the example of Switzerland, it is, in principle, applicable to any region.

Despite large modelling efforts over the recent years and substantial improvements in the understanding of local processes and impacts related to climate change, future climate projections are still associated with large uncertainties. While there has been substantial progress in the characterisation of these uncertainties (Knutti *et al*., 2008), less progress has been reached to reduce them (Mearns, 2010). Uncertainties in climate change projections originate conceptually from three main sources: (1) uncertainty in future anthropogenic emission pathways of greenhouse gases (GHG) and aerosols ('emission uncertainty'), (2) uncertainty in process understanding and its limited representation by climate models ('model uncertainty'), and (3) uncertainty arising from natural fluctuations that are independent from radiative forcing ('natural variability' or 'internal variability') (Cox and Stephenson, 2007). The relative importance of these three main contributions depends on lead time, length of the time intervals considered, region, season, spatial scale, and parameter of interest. For instance, natural variability is particularly large (in relative terms) for near-term projections of precipitation on regional scales, while scenario uncertainty dominates for temperature projections for the end of the century (Cox and Stephenson, 2007; Hawkins and Sutton, 2009, 2011).

These three sources of uncertainty need to be considered when calculating climate change scenarios. Internal variability can be sampled through an ensemble of different model initialisations (Stott *et al*., 2000) or by filtering approaches (Hawkins and Sutton, 2009). Emission uncertainty is typically addressed by conditioning the projections on a limited number of emission scenarios. A common and pragmatic way to address model uncertainty is given by the concept of multi-model combination (Tebaldi and Knutti, 2007; Weigel *et al*., 2008), i.e. by the joint assessment of multiple climate models that should be structurally independent. In reality, different models share similar structural assumptions (Masson and Knutti, 2011) and, in particular, they share similar 'unknown unknowns' in terms of process understanding, so that one is typically left with a limited set of model projections which likely fail to sample the full uncertainty space (Knutti *et al*., 2010). Any uncertainty estimate obtained from a set of model projections is therefore necessarily conditioned on several (subjective) assumptions, ranging from assumptions concerning model independence to assumptions concerning the future behaviour of systematic model biases. To treat this kind of conditional uncertainty, a Bayesian framework is particularly appealing, since it allows decomposing the complex interrelationships between observations, model projections, and unavoidable (subjective) prior assumptions in a systematic and transparent way. A Bayesian approach is also the method of choice in the present contribution.

The basis of this paper is the recently developed Bayesian multi-model combination algorithm described in Buser *et al*. (2009), which is an extension of the work by Tebaldi *et al*. (2005). It is applied here to obtain probabilistic projections of temperature and precipitation. While the algorithm not only considers changes of the mean signal but also changes of the inter-annual variability, we restrict our analysis to changes in the climate mean where the level of scientific understanding is reasonably high. The algorithm of Buser *et al*. (2009) has the specific advantage that it explicitly considers systematic model biases. In particular, it provides three options of how these biases may change in future: (1) model biases are constant with time ('constant bias'), (2) model biases change linearly with time, depending on how well the models reproduce inter-annual variability during the control period ('constant relationship'), and (3) a mixture of these two assumptions as published in Buser *et al*. (2010a). Bias assumption, i.e. the constant bias assumption, is applied in most published climate scenarios in literature (e.g. IPCC, 2007) and it will also be used in the present study. It is important to stress that the other bias assumptions may be equally justified, with potentially significant impact on the outcomes (Christensen *et al*., 2008; Buser *et al*., 2009; Buser *et al*., 2010a).

The algorithm of Buser *et al*. (2009, 2010a) has several other methodological limitations in that it assumes that (1) the input data are normally distributed, (2) the model data are uncorrelated between different models, and (3) there is no internal variability. Here, we provide several pragmatic approaches to overcome each of these limitations, so that this contribution can also be considered as a methodological extension of the algorithm of Buser *et al*. (2009, 2010a). Each of these extensions is

associated with methodological challenges that we will address in the paper in greater detail. To illustrate the performance of the adapted Bayesian approach, the algorithm is finally applied to RCM projections from the ENSEMBLES project to produce a new set of probabilistic climate change scenarios over the 21st century for three distinct climatic regions in Switzerland.

The paper is structured as follows: Section 2 introduces the model and observational data and their temporal and spatial aggregation. It also evaluates the models in how they reproduce observed climate over Switzerland during the control period. The methodological chain applied to calculate probabilistic scenarios is detailed in Section 3. This encompasses an introduction to the Bayesian algorithm as well as data processing steps to be carried out before and after its application. Section 4 presents the obtained results of probabilistic temperature and precipitation scenarios, which is followed by a discussion (Section 5). Summary and conclusions are provided in Section 6.

2. Data source and model validation

2.1. Model data

We make use of projections from the ENSEMBLES RCMs (research theme RT2B in van der Linden and Mitchell, 2009) that were driven by different coupled atmosphere–ocean general circulation models (GCMs). Altogether, a suite of 8 GCMs and 11 RCMs was employed, yielding an ensemble of 20 dynamically downscaled regional climate projections for Europe at a horizontal resolution of 25 km (*Figure 1*). Note that we have excluded the RCM-GCM chain 'HIRHAM (DMI)' driven by 'BCM (NERSC)', as a serious simulation error was reported by DMI at the time of the analysis. The 20 RCM-GCM simulations were conducted in transient mode following the Intergovernmental Panel on Climate Change (IPCC) A1B emission scenario (Nakicenovic and Swart, 2000) and covering at least the time period 1950–2050. A subset of simulations (14 RCM-GCM chains with 6 GCMs involved) was run beyond 2050 to cover the full 21st century. Owing to limited computational resources, not every combination of a driving GCM and a downscaling RCM could be simulated. In fact, the RCM-GCM combination matrix (in table V.1 in van der Linden and Mitchell, 2009) reveals considerable gaps and unequal numbers of RCMs per driving GCM. Note that one GCM (HadCM3) has been applied in three parameter configurations corresponding to a low, standard, and high climate sensitivity. These three configurations represent a subset of a larger ensemble, namely the METO-HC GCM-perturbed physics ensemble (Murphy *et al.*, 2004 give more details on the approach). In terms of their correlation structure and projection characteristics over the Alpine domain, these three model configurations can be interpreted as three independent GCMs, at least for the purpose of the present study.

2.2. Observational data

Our primary source of observational reference data is the ENSEMBLES gridded observational dataset for precipitation and temperature (referred to as 'E-OBS' henceforth) in monthly resolution. This includes data from a heterogeneous station network, which has been interpolated onto the same 25 × 25 km rotated pole grid that is used for the RCM integrations, thus making it particularly suitable for the validation of the ENSEMBLES RCM simulations (Haylock *et al.*, 2008). We used version 3.0 of the dataset that spans the period 1950–2009

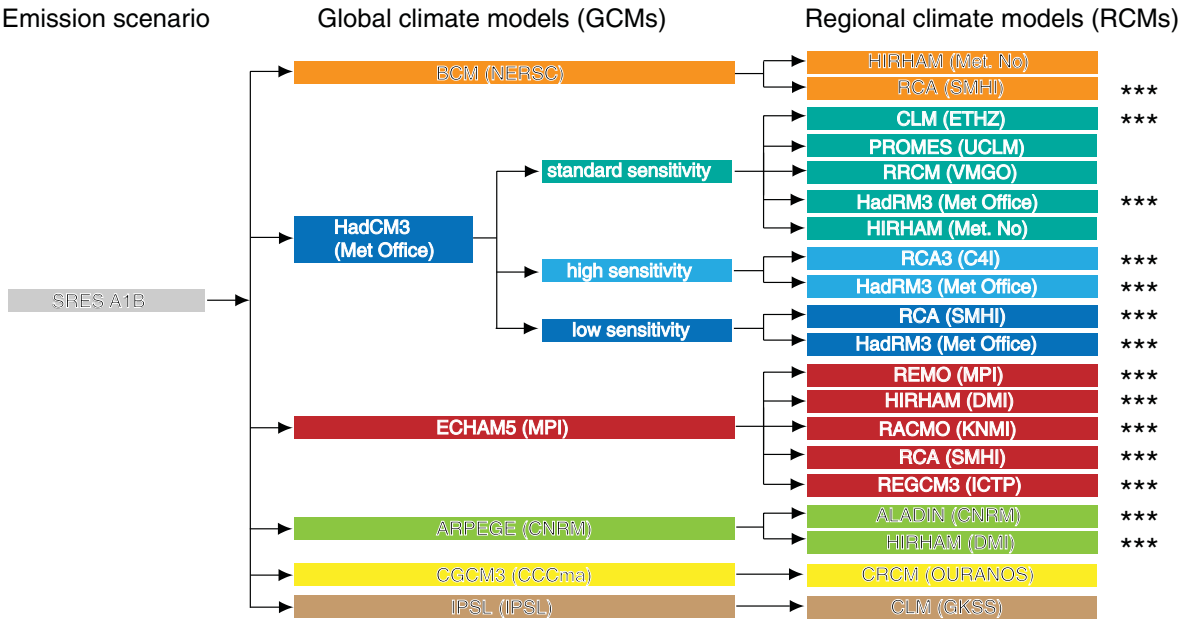

Figure 1. ENSEMBLES RCM-GCM chains (colour coded according to driving GCM) used for the study. Asterisks behind bars mark those simulations that run until 2100. Note that the GCM HadCM3 is run in three sensitivity configurations. The abbreviations in brackets denote the main centre responsible for the corresponding model simulation.

(available at: http://eca.knmi.nl/). Note that limitations of the dataset have been unveiled recently that mainly concern the data in daily resolution (e.g. Hofstra *et al*., 2010; Kysely and Plavcova, 2010). Monthly or even seasonally aggregated data are not strongly affected by these limitations.

To quantify internal variability of the observed climate in Switzerland (detailed in Section 3.1.1.), we used homogenized station data from MeteoSwiss (Begert *et al*., 2005) that go back to 1860.

2.3. Temporal and regional aggregation

The 20 RCM-GCM chains employed in this study provide data output in daily resolution for grid cells of 25 km width. To enhance the statistical robustness of the projections, the output of each model chain as well as the observational data have been aggregated to seasonal and regional averages. In terms of temporal aggregation, the following seasons have been considered: December–February (DJF), March–May (MAM), June–August (JJA) and September–November (SON). In terms of spatial aggregation, climatologically similar grid points were aggregated into three Swiss regions of similar size as shown in *Figure 2*: northeastern Switzerland (CHNE), western Switzerland (CHW), and Switzerland south of the Alps (CHS). The spatial extent of these three regions was determined semi-empirically on the basis of the spatial correlation structure of temperature and precipitation. First, three core regions in northeastern, western and southern Switzerland have been defined (black dots in the two lower rows of *Figure 2*). Then, for each season, each model (including the E-OBS data), and each variable (precipitation and temperature), the seasonal averages of these core regions have been correlated with the seasonal averages of the surrounding grid points. On the basis of this procedure, grid points could be identified which are climatologically similar to the core regions, and which can, therefore, be used to extend the core regions to enhance statistical robustness. This procedure includes grid points outside of Switzerland. As an example, the correlation patterns for E-OBS, averaged across all four seasons, are shown in *Figure 2*. In general, correlations of temperature are much higher than in case of precipitation, where the values drop rapidly with distance from the core region. Temperature remains highly correlated across the Swiss plateau north of the Alps, and in a rotated U-shape pattern along the southern side. By analysing the correlation structures, the regions CHNE, CHW, and CHS have been defined as presented in the top row of *Figure 2*. Since the correlation patterns vary between models (including E-OBS), seasons, and variables, the exact definition of the regions CHNE, CHW and CHS represents an ultimately subjective compromise

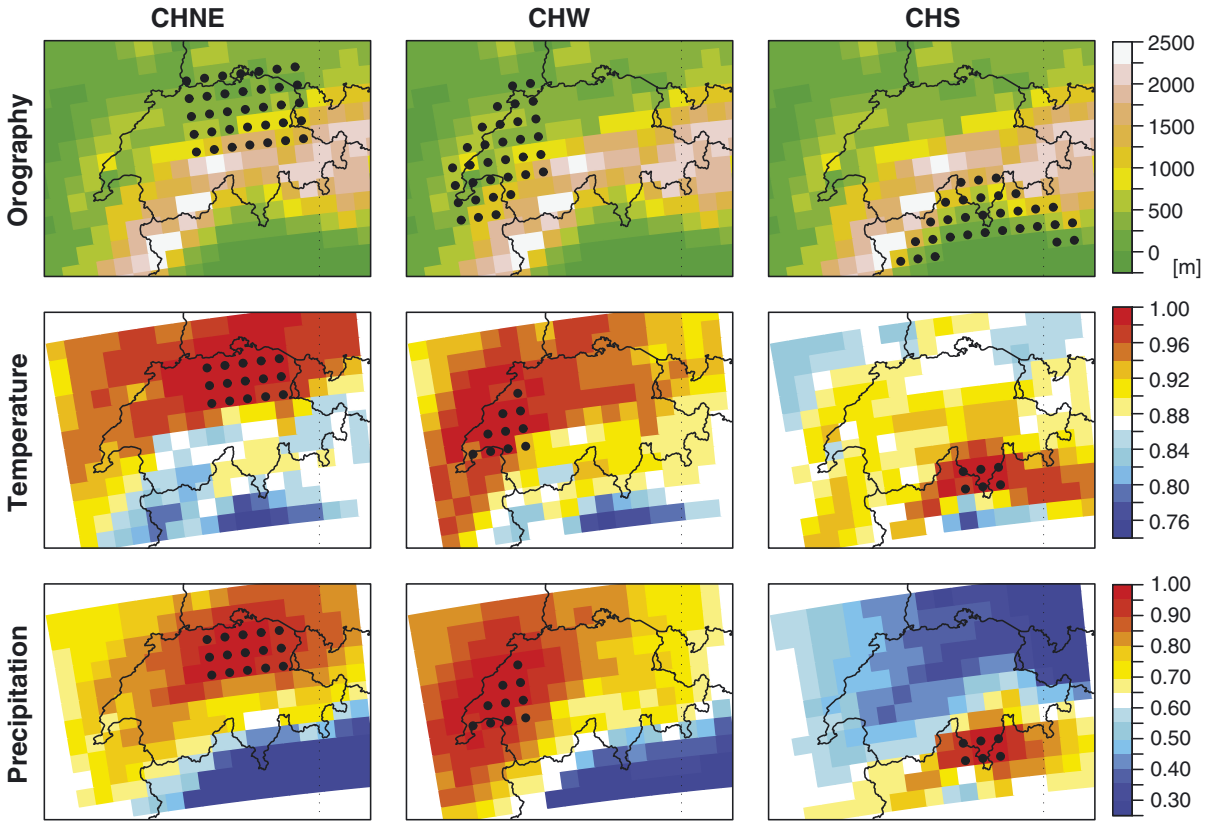

Figure 2. Upper row: Spatial extent of the three different regions that are mapped onto the grid and topography of E-OBS for illustration. Middle and lower rows: At each grid cell, the correlation with the spatial average of the core region is shown for seasonal temperature (middle row) and for seasonal precipitation (lower row). The core regions are marked with black symbols. Shown are the correlation coefficients averaged across the four seasons in E-OBS.

between the different correlation maps obtained for each season, variable, and model. The three final regions have been defined such that they have about the same number of grid points (31 in CHS, 33 in CHW, and 35 in CHNE) and, hence, a comparable sampling uncertainty. The high-elevation Alpine region has been excluded from the analysis, since (1) averaging the highly localized and complex nature of Alpine climate is not meaningful, and (2) the RCMs suffer from representing the complex topography realistically. For instance, the height of the peak model Alpine topography is substantially lower than in reality (e.g. Ceppi *et al*., 2010).

The scenarios are intended to provide information on climatic changes over the 21st century with respect to a reference period characterizing present climate. As a reference period, the 30-year interval 1980–2009 has been chosen. As scenario periods, the three 30-year intervals 2020–2049, 2045–2074, and 2070–2099 have been considered. For simplicity, throughout the study, these periods are denoted with the corresponding central year of the time window (i.e. 2035, 2060, and 2085).

2.4. Model evaluation

An in-depth assessment of the performance of the ENSEMBLES models is beyond the scope of this study. Here, the ability of the models to reproduce the annual cycle of seasonal mean temperature and precipitation over the three Swiss regions is inspected. *Figure 3* shows seasonal mean temperature and precipitation as simulated by the 20 RCM-GCM model chains, and from E-OBS for the three regions defined above during the reference period. The models simulate temperature reasonably well in terms of the qualitative reproduction of the annual cycle. In absolute terms, considerable biases are observed in the range of about −5 and +2 K (5–95% quantile of the model ensemble). For the annual cycle in precipitation, biases are in the range between −15 and 145% relative to the corresponding E-OBS values (5–95% quantile of the model ensemble). The majority of the models have a tendency to be too cool and too wet. This is in good agreement with the findings of Kjellström *et al.* (2010). However, the ranges are markedly larger than those reported by Jacob *et al*. (2007) for the model chains of the PRUDENCE project (a predecessor project of ENSEMBLES) over the Alpine region (between around −2.5 and +2 K for temperature, and between −35 and +25% for precipitation). While the smaller biases in the older PRUDENCE project may appear paradoxical at first sight, this discrepancy can likely be explained by the following reasons: Biases in RCM-GCM chains are to a large degree directly related to errors in the representation of the large-scale circulation in the GCMs and in particular to biases in the simulation of sea surface temperatures (SSTs) and sea-ice cover (Kjellström *et al*., 2010). For the control period, the PRUDENCE simulations were run using prescribed observational SSTs and sea-ice cover data, while the ENSEMBLES GCMs were coupled to a free-running ocean model. This implies substantially reduced biases in the large-scale circulation of the PRUDENCE models. An additional reason could be the smaller size of the evaluation domain in the present study.

As can be seen from *Figure 3*, within the set of ENSEMBLES models, we also encounter models with exceptionally large biases. For instance, one RCM-GCM chain exhibits temperature biases of more than 7 K (in spring over all regions) while another chain simulates precipitation 3.5 times, and in one case even 6 times larger than E-OBS (over CHS during winter). The reasons for these particularly large systematic errors in these two chains (with potentially large impacts on the modelled local physics) remain unclear, but their investigation lies beyond the scope of this study.

Despite the obvious existence of large systematic biases, none of the 20 model chains has been excluded from the ensemble, nor have the models been weighted according to their skill. This is for three reasons: Firstly, none of the models performs consistently bad over all aspects of the validation. For instance, those models which perform worst in terms of precipitation perform reasonably well in terms of temperature. Secondly, those models revealing large biases during the control period behave inconspicuously in terms of their projected climate change signal. This is consistent with the fact that, at present, it is not known how, or whether at all, metrics of global model performance during the control period correlate with future model projections (Räisänen, 2007;

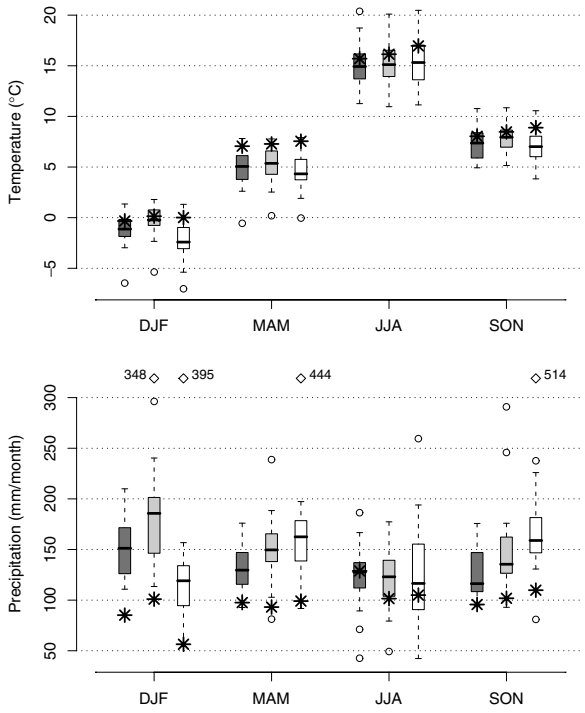

Figure 3. Boxplots of seasonally averaged temperature (precipitation) in the upper (lower) panel obtained from 20 RCM-GCM chains over the region of CHNE (dark grey), CHW (light grey), and CHS (white) for the reference period 1980–2009. The observations from E-OBS are marked with an asterisk symbol. Diamonds in the lower panel are outliers outside the axis range with the respective mean values noted aside the symbols.

Knutti *et al.*, 2010). Third, a recent conceptual study has shown that uncertainties in the weights applied to the individual models may lead to multi-model projections which have lower skill than if no weights had been applied at all (Weigel *et al.*, 2010).

3. Methods: Derivation of probabilistic scenarios

The core of our methodology is the recently developed Bayesian algorithm of Buser *et al.* (2009) (in the following referred to as 'BAB') – an algorithm which allows the joint assessment of multiple model output in a probabilistic framework. The algorithm combines observational data with model simulations of past and future climate, yielding probabilistic projections of expected changes in seasonal mean temperature and precipitation. It is described in Section 3.2. Despite its conceptual elegance, the applicability of the BAB to the ENSEMBLES GCM-RCM chains is associated with three constraints: Firstly, the BAB requires that the data are normally distributed, which is not necessarily the case in reality (e.g. for precipitation). Secondly, the BAB requires that data stemming from individual RCM-GCM chains are independent from each other, which is not the case if several RCMs have been driven by the same GCM. Thirdly, the BAB assumes that the disagreement between individual model projections is entirely due to model uncertainty, thus ignoring the fact that model discrepancies may also be due to internal variability. These constraints require the application of several pragmatic pre-processing (Section 3.1.) and post-processing (Section 3.3.) steps so that the algorithm becomes applicable to ENSEMBLES model data. These steps are explained in what follows.

A schematic illustration of the entire processing chain is provided in *Figure 4*. The order of the sections and subsections follows the order of the processing stages of the data. More specifically, the following steps are undertaken: First, since internal variability is not explicitly considered within the algorithm, it is removed from the original time series by a filtering approach prior to model combination (Section 3.1.1.) and then added to the posterior projections after the Bayesian multi-model combination has been carried out (Section 3.3.2.). Second, to ensure that input data are normally distributed, an appropriate transformation is applied where required (Section 3.1.2.), and the posterior distribution is retransformed accordingly (Section 3.3.1.). Finally, the independence requirement of model data can be partly satisfied by averaging those RCM simulations driven by the same GCM (Section 3.1.3.). The BAB itself is described in Section 3.2.1. Of central importance for the application of the BAB is the specification of prior assumptions concerning the magnitude of model uncertainty (Section 3.2.2.).

While the ENSEMBLES regional climate projections have only been calculated for the A1B emission scenario, this study also seeks to provide information for other emission scenarios. These are obtained from the A1B scenarios by the technique of pattern scaling. Section 3.4. provides a description of this technique, and how it is integrated into the processing chain described in Sections 3.1.–3.3.

The entire processing chain described in the following is applied separately to each season (DJF, MAM, JJA, SON), each region (CHNE, CHW, CHS), each variable (temperature and precipitation), and each scenario period (2035, 2060, 2085), taking 1980–2009 as reference. In total, this results in 72 independent probabilistic estimates of climate change for the A1B emission scenario. Strictly speaking, each of the variables introduced in the following should therefore be supplied with indices for scenario period, season, and region. However, for better readability these are omitted henceforth. Note that, in practice, the regions, seasons and variables are not fully independent. At the example of PRUDENCE simulations, Buser *et al.* (2010b) extended the BAB to also project changes in the combined distribution of temperature and precipitation.

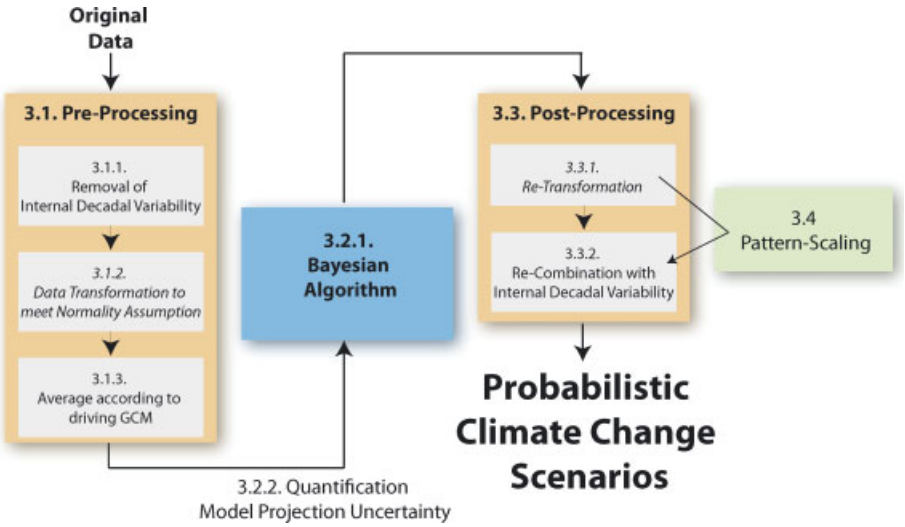

Figure 4. Schematic overview of the methodology detailed in Section 3. The numbers indicate the corresponding sections. The steps denoted in italics only apply to precipitation data.

Yet, a robust quantitative assessment of the change in the correlation structure is difficult due to the small number of independent GCMs available.

3.1. Pre-processing of data

The starting point of the processing chain are seasonal and regional averages of model output and observation data. In the following, $\hat{X}^{(0)}_{0,t}$ denotes the seasonal-regional average of the E-OBS observations in year t, while $\hat{X}^{(0)}_{m,t}$ is the seasonal-regional average of the output of model m in year t. For the former, t can only assume values in the past, while for the latter t can assume values both in the past and in the future. The hat $(\wedge)$ symbolizes pre-processed data (i.e. before application to the Bayesian algorithm). The superscript (0) indicates that these are raw data which have not yet been further processed. By construction, the BAB requires that the input data (i.e. regional-seasonal averages of observations and model output) are: (1) free of internal variability, (2) normally distributed, and (3) independent. These criteria have been checked beforehand and, where necessary, appropriate adjustments have been applied to the data, i.e. to $\hat{X}^{(0)}_{0,t}$ and $\hat{X}^{(0)}_{m,t}$. To facilitate the discussions to follow, the superscript index of the data is incremented by 1 for each processing step described in the following (i.e. '*(1)*' in Section 3.1.1., '*(2)*' in Section 3.1.2., and '*(3)*' in Section 3.1.3.). Also note that, as illustrated in *Figure 4*, some pre-processing steps are complemented by corresponding post-processing steps applied to the posterior distributions obtained from the BAB (Section 3.3.).

3.1.1. Internal variability

The BAB makes the implicit assumption that changes in climate mean are not affected by internal variability, an assumption which is not consistent with reality (Hawkins and Sutton, 2009). To circumvent this inconsistency, we remove the internal variability component from E-OBS and the 20 RCM-GCM chains beforehand, and add the variability component again after applying the BAB.

Following Hawkins and Sutton (2009), we decompose the time series of temperature and precipitation ($\hat{X}$) for each RCM-GCM chain (m), and E-OBS *(0)* into a slowly varying component representing anthropogenic climate change (x), and the remaining fluctuations representing year-to-year variability and other internal variability such as decadal oscillations (ε)

$$\begin{aligned} \hat{X}^{(0)}_{0,t} &= x_{0,t} + \varepsilon_{0,t} \\ \hat{X}^{(0)}_{m,t} &= x_{m,t} + \varepsilon_{m,t} \end{aligned} \qquad \textbf{(1)}$$

Again, the superscript '(0)' indicates that original data are not yet processed. As in Hawkins and Sutton (2009), the slowly varying components $x_{m,t}$ and $x_{0,t}$ have been determined by a fourth-order polynomial fit to the times series of observations $\hat{X}^{(0)}_{0,t}$ and model data $\hat{X}^{(0)}_{m,t}$, respectively.

The fit reflects in our case the atmospheric long-term response to perturbations in the Earth's radiation balance. For E-OBS, the fit is estimated over the time span 1950–2009 and for the models from 1955 up to the end of the simulation, i.e. to 2050 for the unstarred models in *Figure 1*, and to 2099 for the starred models in *Figure 1*. An example of such a polynomial fit is shown in *Figure 5*(a) for the model chain CLM-HadCM3Q0. Since the climate change scenarios in the BAB are constructed from a reference and a scenario period of 30 years each, we need to account for the effects of natural variability on exactly this time scale. This is done by a two-step procedure: First, the natural fluctuations on the 30-year scale are calculated by applying a 30-year moving average on the annual fluctuations ε, yielding time series $< \varepsilon_{m,t} >_{30yr}$ and $< \varepsilon_{0,t} >_{30yr}$ as illustrated in *Figure 5*(b). For simplicity, the variability of these 30-year fluctuations is henceforth referred to as decadal variability. As a second step, these 30-year fluctuations are then subtracted from the original time series, yielding new data time series $\hat{X}^{(1)}_{0,t}$ and $\hat{X}^{(1)}_{m,t}$ which lack decadal variability (illustrated for 1980–2009 in *Figure 5*(c), red curve)

$$\begin{aligned} \hat{X}^{(1)}_{0,t} &= x_{0,t} + \varepsilon_{0,t} - < \varepsilon_{0,t} >_{30yr} \\ \hat{X}^{(1)}_{m,t} &= x_{m,t} + \varepsilon_{m,t} - < \varepsilon_{m,t} >_{30yr} \end{aligned} \qquad \textbf{(2)}$$

Note that, by doing so, we implicitly assume that the decadal variability (in absolute terms) does not depend

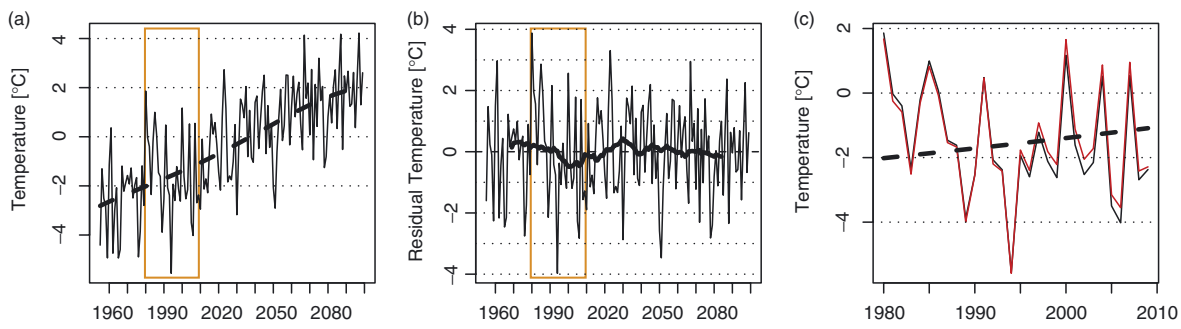

Figure 5. Winter temperature (in °C) over CHNE for the CLM-HadCM3Q0 model chain. (a) Raw data (thin line) together with a 4th-order polynomial fit (bold dashed line) over 1955–2100; (b) Residuals as output from the regression model (thin line) and filtered with a 30-year moving average (bold solid line); (c) model time series original (black) and after removing the internal decadal variability (red) over the time window 1980–2009. The time window has been reduced here for illustrative purposes. It is displayed in orange in the left and middle panels.

on the lead time and hence remains constant over the full simulation period. Also note again that the decadal variability removed will be added again after model combination (Section 3.3.2.).

How large is decadal variability for the model and observation data applied in this study? *Figure 6(a)* compares the magnitude of the decadal variability of temperature (standard deviation) in all RCM-GCM simulations and observations. Generally, over all three regions, the temperature variability in E-OBS (asterisks) and in the models is largest during winter, reflecting the enhanced dynamical variability on the synoptic scale during this season (e.g. Hurrell and van Loon, 1997; Ceppi *et al*., 2010). Variability estimates differ between models particularly for summer (∼0.05–0.25 K), when convective processes and land–surface atmosphere interactions become important. Overall, the obtained estimates of decadal temperature variability seem to be consistent with estimates by Hawkins and Sutton (2009), who reported a value of 0.16 K for the modelled European mean temperature filtered with 20-year moving averages.

Figure 6(b) shows the corresponding comparison for precipitation. For E-OBS, no distinct annual cycle that is common to all three regions is observed. Considering the three regions and four seasons (note the different vertical axis for CHS), variability is smallest over CHW during summer (∼1 mm/month) and largest for spring and autumn over CHS (close to 3 mm/month). Expressed as percentage of seasonal mean precipitation, the decadal variability within E-OBS varies between around 1 and 3%, which is again consistent with Figure 8 in Hawkins and Sutton (2011), given that they analyse 10-year averages but over a much larger domain. The decadal variability of the ENSEMBLES models does not exhibit a pronounced annual cycle either, but shows minima in summer over CHW and CHS, just as the observations. Differences among the models are largest during DJF and some positive outlier models (with values up to 4–5 times bigger than E-OBS) are apparent in all regions.

Generally, the decadal variability of E-OBS is at the lower end of the range of variability estimates among the models. This is particularly true for temperature but also for precipitation in all seasons and regions. This discrepancy between models and E-OBS could, at least partially, be an effect of fitting a polynomial to a much shorter time series in case of E-OBS (1950–2009). For this reason, we made the same analyses using homogenized station observations that go back to 1864 (Begert *et al*., 2005). To represent the region of CHW (CHNE) we averaged the two stations, Berne and Geneva (Basel and Zurich), and used the single station of Lugano for CHS. As shown in *Figure 6*(a) and (b), the decadal variability estimates of these long-term time series (marked by triangles) are larger than in E-OBS and, in general, lie near the centre or at the upper end of the model regional ensemble (exceptions are winter precipitation in all regions and summer precipitation over CHNE and CHW). Besides the aforementioned fitting effect due to the longer time series, this higher decadal variability may also partially be attributed to the fact that only one or two single stations have been analysed instead of a regional average as in E-OBS. This may

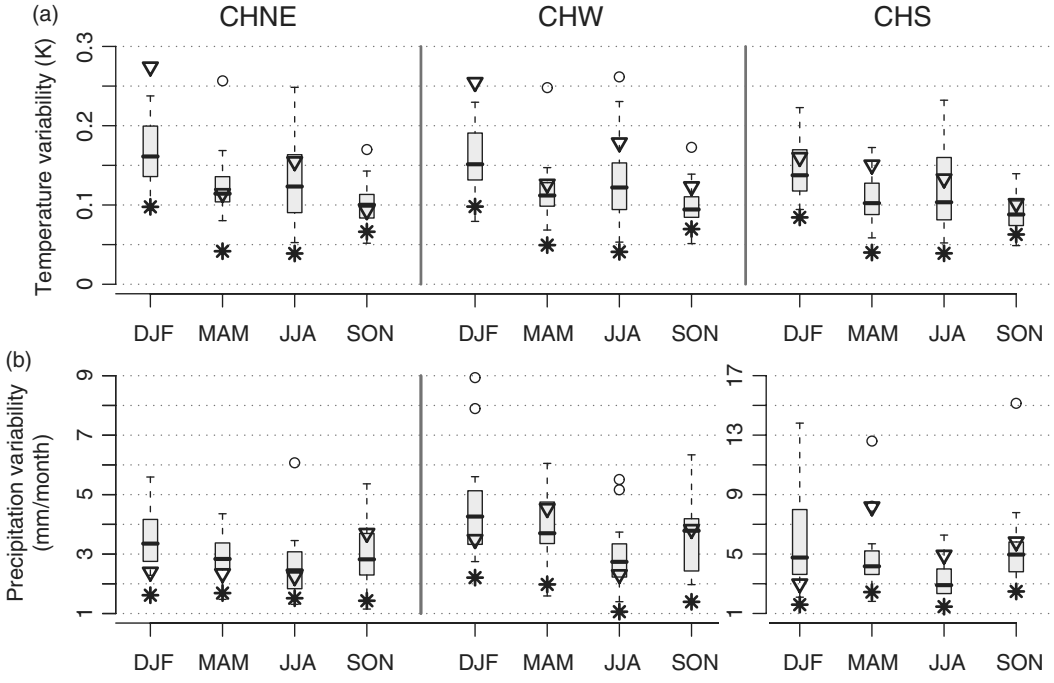

Figure 6. (a) Annual cycle of internal decadal variability of temperature (standard deviation) in 20 individual RCM-GCM chains (boxplots), E-OBS observation (asterisks) and representative station observations (triangles). The station observations represent the average of two selected stations in CHNE and CHW, and one selected station in CHS. Note that model and E-OBS data are averaged over the regions CHNE, CHW, and CHS. (b) is as (a), but for precipitation. Note the different axis on the right hand side for precipitation over CHS.

be particularly relevant for precipitation where spatial correlations between the selected meteorological stations are generally lower and the effect of regional averaging thus larger than for temperature. Note that the increase in variability is not seasonally uniform, leading also to differences in the qualitative shape of the annual cycle as compared to E-OBS.

3.1.2. Normal distribution and autocorrelation

As will be discussed more in detail in Section 3.2.1., the input data into the BAB are observed and modelled regional–seasonal averages of temperature and precipitation during the control period, and modelled regional–seasonal averages during the scenario periods. Within each of these 30-year intervals, the BAB requires that (1) the data are normally distributed, and (2) that they have no year-to-year autocorrelation. To check the autocorrelation condition, lagged correlations coefficients have been tested (at the 5% significance level) against the null-hypothesis of a normal distribution with zero mean and variance $1/N$, where N represents the sample size (Chatfield, 2004). Since the null-hypothesis could not be rejected, the modelled and observed temperature and precipitation time series are treated as not autocorrelated, implying that no further adjustments to the data are necessary in this respect.

To test whether the data are normally distributed, we applied the Shapiro-Wilks test on each 30-year set of data values considered. For temperature, the normal assumption holds for almost all models and seasons. Hence, a transformation is not necessary, and we have

$$\hat{X}^{(2)}_{0,t} = \hat{X}^{(1)}_{0,t} \text{ and } \hat{X}^{(2)}_{m,t} = \hat{X}^{(1)}_{m,t} \tag{3}$$

Precipitation data, on the other hand, have been found to be often positively skewed. To find the optimal transformation for precipitation data, we performed several box-cox transformations (Box and Cox, 1964) iterating over a range of lambda parameters. A simple square root transformation leads in most cases to data which are sufficiently normal. Moreover, due to the considerable biases of modelled precipitation (*Figure 3*), and due to the fact that modelled precipitation variance often scales with precipitation bias, the raw model data are linearly scaled such that their means during the control period are identical to the observational means. This facilitates the further processing steps significantly. Hence, the precipitation data after this second pre-processing step have the following format:

$$\hat{X}^{(2)}_{m,t} = \sqrt{\hat{X}^{(1)}_{m,t} \cdot \frac{< \hat{X}^{(1)}_{0,1980-2009} >}{< \hat{X}^{(1)}_{m,1980-2009} >}}$$

$$\hat{X}^{(2)}_{0,t} = \sqrt{\hat{X}^{(1)}_{0,t}} \tag{4}$$

with $< \hat{X}^{(1)}_{m,1980-2009} >$ and $< \hat{X}^{(1)}_{0,1980-2009} >$ being mean observed and modelled precipitation during the reference period.

3.1.3. Inter-model correlations

Independence between data stemming from different models is another requirement of the BAB. This requirement is violated by construction, since several RCMs are driven by the same GCM and hence highly correlated (see also Kjellström *et al*., 2010). One option to circumvent this problem is to only consider a subset of the available model chains, such that only one RCM per driving GCM is taken (Buser *et al*., 2010a). Here a different approach has been chosen which allows all available ENSEMBLES RCM-GCM chains to be included in the evaluations: Independence is obtained by simply averaging all RCMs that have been driven by the same GCM. This pre-processing step then yields both for temperature and precipitation

$$\hat{X}^{(3)}_{i,t} = \frac{\sum_{m=1}^{n_i} \hat{X}^{(2)}_{m,t}}{n_i} \tag{5}$$

Here, variable 'n_i' denotes the number of RCMs driven by the i-th GCM. Note that this averaging procedure reduces the number of independent model datasets fed into the BAB to an ensemble of 8 (6) simulations up to 2050 (beyond 2050). In the following, these averaged simulations are indexed by letter 'i'. It should be noted that aggregating RCMs according to driving GCM does not fully resolve the model independence problem. This is for two reasons: (1) Many GCMs have similar structures and similar biases, and are based on similar parameterisations of unresolved processes (e.g. Masson and Knutti, 2011). (2) In the ENSEMBLES matrix, in some cases, the same RCM (e.g. 'RCA' model) is driven by several GCMs (*Figure 1*). In addition, the aggregation removes some of the inter-model RCM spread that is particularly relevant during the summer season.

3.2. Bayesian algorithm of Buser *et al*. (2009)

3.2.1. Formulation of the Bayesian algorithm

For details on the BAB, the reader is referred to the paper of Buser *et al*. (2009). Here, only a summary is provided. The BAB generates probability distributions of various climatic parameters of interest, Θ, conditioned on the data available: $p(\Theta|Data)$. 'Data' here, refers to observation data during the reference period, and model data during the reference and scenario periods, while Θ refers to a set of parameters characterizing the data (e.g. model bias and climate mean shift). The BAB computes $p(\Theta|Data)$ on the basis of the Bayes theorem, which states that $p(\Theta|Data)$, i.e. the posterior distribution, can be formulated as a product of the likelihood $p(Data|\Theta)$ and the prior distribution of the parameters, $p(\Theta)$:

$$p(\Theta|Data) \propto p(Data|\Theta) \times p(\Theta) \tag{6}$$

As high-dimensional distributions are involved, the computation of the posterior density for a single parameter

cannot be performed analytically but relies on approximative sampling techniques (Markov Chain Monte Carlo techniques; Gilks *et al.*, 1996). In the present study, a so-called Gibbs-sampler has been applied in the configuration as described in Buser *et al.* (2009).

As 'Data', we use our pre-processed time series of Section 3.1. (i.e. $\hat{X}_{0,t}^{(2)}$, $\hat{X}_{i,t}^{(3)}$). For simplicity, in the following, the superscript '*(2)*' and '*(3)*' are omitted. To be consistent with the notation of Buser *et al.* (2009), $X_{0,t}$ and $X_{i,t}$ are henceforth only used to describe observation and model data (seasonal averages of temperature and precipitation) during the *reference period*, with $t = 1, \ldots 30$ indexing the respective year within the 30-year reference period (1980–2009). To denote model data and (unknown) 'observation' data during the *scenario period*s, $Y_{i,t}$ and $Y_{0,t}$ are used, where $t = 1, \ldots 30$ is the index of the respective year within the 30-year scenario period considered. Index i denotes the different driving GCMs. One has $i = 1, \ldots 8$ for the short-term scenario period (2035), and $i = 1, \ldots 6$ for the medium and long-range scenario periods (2060 and 2085, respectively). It is assumed that $X_{0,t}$, $X_{i,t}$, $Y_{0,t}$, and $Y_{i,t}$ are normally distributed and independent (Sections 3.1.2. and 3.1.3.). To keep the notation simple, it is in the following assumed that the data *within* the reference period and the data *within* the scenario periods have been detrended beforehand. In practice, linear trends within the individual 30-year intervals are modelled by the BAB by means of an explicit trend parameter (Buser *et al.*, 2009).

Following the notation of Buser *et al.* (2009), the **likelihood** $p(Data|\Theta)$**,** i.e. the distribution of model and observational data given the climatic parameters, is modelled as follows:

$$\begin{aligned} X_{0,t} &\sim \mathcal{N}(\mu, \sigma_{X_0}^2) \\ X_{i,t} &\sim \mathcal{N}(\mu + \beta_i, \sigma_{X_i}^2) \\ Y_{0,t} &\sim \mathcal{N}(\mu + \Delta\mu, \sigma_{Y_0}^2) \\ Y_{i,t} &\sim \mathcal{N}(\mu + \beta_i + \Delta\mu + \Delta\beta_i, \sigma_{Y_i}^2) \end{aligned} \qquad \textbf{(7)}$$

where $\sim \mathcal{N}(\mu, \sigma^2)$ means 'randomly sampled from a normal distribution with mean μ and variance σ^2'. The statistical model in Equation (7) is specified by several parameters describing central tendency and year-to-year variability of the data. μ is the central tendency of the observed climate during the reference period, $X_{0,t}$. As outlined above, models are subject to systematic biases and the central tendency of the model data during the reference period, $X_{i,t}$, may be shifted with respect to μ. This model-dependent shift is modelled by an error term β_i. As has been mentioned above, it is here assumed that β_i stays constant with time ('constant bias assumption'), but other options are, in principle, possible (Buser *et al.*, 2009; Buser *et al.*, 2010a). The distribution of future observations ($Y_{0,t}$), which, of course, are not yet known, is assumed to be shifted by a climate change signal $\Delta\mu$ with respect to μ, so that the distribution of $Y_{0,t}$ is centred at $\mu + \Delta\mu$. It is this climate change parameter $\Delta\mu$ which is of most interest for the study here. If the participating climate models were perfect (apart from a systematic bias β_i), the future model projections ($Y_{i,t}$) should be centred at $\mu + \Delta\mu + \beta_i$. In reality, however, different climate models are subject to different assumptions and errors and have different climate sensitivities, so that they react differently to changes in greenhouse gas concentrations. In Equation (7) this is modelled by an additional model-dependent error term $\Delta\beta_i$, which can be interpreted as 'model projection errors' (note that the sum $\Delta\mu + \Delta\beta_i$ represents the expectation value of $Y_{i,t} - X_{i,t}$). In fact, these model projection errors represent an important contribution to the still substantial uncertainties inherent to the generation of climate scenarios (referred to as 'model uncertainty in Section 1.).

Similar to the central tendencies, the inter-annual variabilities $\sigma_{X_0}^2$, $\sigma_{X_i}^2$, $\sigma_{Y_0}^2$, $\sigma_{Y_i}^2$ can be decomposed into parameters describing the observed inter-annual variability during the reference period, systematic model biases, climate change signal, and projection errors. However, since inter-annual variability is not further evaluated in this study, the reader is referred to Buser *et al.* (2009) for a detailed discussion on these parameters.

Note that the BAB inherently assumes that any differences between observed and modelled climate means are exclusively due to bias and projection error terms β_i and $\Delta\beta_i$. However, in reality some of these discrepancies may also be due to internal decadal variability, i.e. natural variations of the central tendencies of observed and modelled climate. Here, this conceptual deficiency of the BAB has been circumvented pragmatically by subtracting internal variability prior to applying the BAB (Section 3.1.1.), and re-adding it after Bayesian model combination (Section 3.3.2.). A formal extension of the BAB to directly account for internal variability is left for future research. Among other changes, this would require that the likelihood is extended by a further additive parameter describing these natural fluctuations in observations and individual models separately.

To calculate the posterior distributions of each of the parameters of interest (in particular, $\Delta\mu$), the BAB requires that **prior distributions** are specified for all parameters. For the prior distributions of the additive parameters, i.e. $p(\mu)$, $p(\Delta\mu)$, $p(\beta_i)$, $p(\Delta\beta_i)$, the BAB assumes a normal distribution with mean and variance being specified by so-called hyper-parameters. Whenever possible, large values are chosen for the prior variances, so that the priors become essentially flat and non-informative, and the posterior distributions are mainly determined by the likelihood. This strategy works well for the prior distributions of μ, $\Delta\mu$ and β_i. Table I. and II present our choices of the hyper-parameters used for temperature and square root transformed precipitation, respectively. As can be seen, the priors for $X_{0,t}$ are centred close to the observed climatological means. By that, a prior variance of 'only' 25 K$\wedge$2 is wide enough to be considered as non-informative. For the prior distributions of the multiplicative parameters, which are related to year-to-year variability, as well as of the trend

parameters – both of these are not explicitly expressed in Equation (7) – we refer to Table II in Buser *et al.* (2009).

Regarding the projection error term $\Delta\beta_i$ (in Buser *et al.*, 2009 referred to as bias change), the situation is more complicated since an informative prior definition is required. The reason is that only the sum $\Delta\mu + \Delta\beta_i$ is identifiable from the data, but not the two parameters $\Delta\mu$ and $\Delta\beta_i$ alone. In other words, without restricting the variance of the prior for $\Delta\beta_i$, the posterior distribution of $\Delta\mu$ would be uninformative, since any specific value of $\Delta\mu$ could in principle be compensated by a $\Delta\beta_i$ term of similar magnitude but opposite sign (Buser *et al.*, 2009 for a detailed discussion of this identifiability problem). Reasonably sharp posterior distributions of $\Delta\mu$ are only obtained if the model projection errors are, *a priori*, assumed to be within certain bounds. This is a general problem in climate projections, and one is forced to make partly subjective prior assumptions concerning the magnitude of the tolerable model projection errors.

To specify the prior of $\Delta\beta_i$, here we make the following assumptions: (1) the projection errors are centred at zero, implying that positive and negative projection errors are *a priori* considered equally plausible (an assumption, inherent to most published climate projections, e.g. IPCC (2007)); (2) the variance of projection uncertainty is given by a hyper-parameter $\sigma^2_{\Delta\beta}$, which is obtained from the assumption that the projection uncertainty is fully sampled by the available model runs (details in Section 3.2.2.). The prior for $\Delta\beta_i$ is then formally given by

$$\Delta\beta_i \sim \mathcal{N}(0, \sigma^2_{\Delta\beta}) \quad \textbf{(8)}$$

In the following, $\sigma^2_{\Delta\beta}$ is referred to as model projection uncertainty.

Table I. Hyper-parameters for the prior distributions of temperature.

Parameter	Expectation value μ_0 (in °C)	Variance σ_0^2 (in K^2)	95% Confidence interval (in °C)
μ (DJF)	0	25	[−9.8, 9.8]
μ (MAM)	7	25	[−2.8, 16.8]
μ (JJA)	15	25	[5.2, 24.8]
μ (SON)	9	25	[−0.8, 18.8]
$\Delta\mu$	0	16	[−7.8, 7.8]
β_i	0	25	[−9.8, 9.8]

3.2.2. *Quantification of model projection uncertainty*

As already pointed out in Buser *et al.* (2009), the prior assumption of projection uncertainty, $\sigma^2_{\Delta\beta}$, has a strong impact on the uncertainty range in the posterior distribution of climate mean shift $\Delta\mu$. Before outlining how $\sigma^2_{\Delta\beta}$ is chosen in the present study, we first investigate this relationship more in detail by controlled sensitivity experiments, using the BAB with different prior settings of $\sigma^2_{\Delta\beta}$ while keeping the corresponding hyper-parameters for $\Delta\mu$ constant. The analyses are carried out at the example of pre-processed model data ($\hat{X}^{(3)}_{i,t}$) of temperature over the CHNE region. *Figure 7*(a) shows the raw model output and the 95% confidence interval of the posterior distribution of $\Delta\mu$ for projections of winter mean temperature for the three scenario periods and for four different choices of $\sigma^2_{\Delta\beta}$. The width of the confidence intervals increases with larger prior settings (from ∼0.5 K at $\sigma^2_{\Delta\beta} = 0.1$ K^2 to almost 4 K at $\sigma^2_{\Delta\beta} = 7$ K^2), eventually exceeding the range spanned by the available raw model projections. The central tendency of $\Delta\mu$ remains almost unaffected by the choice of $\sigma^2_{\Delta\beta}$, while the uncertainty range is strongly determined by the magnitude of this prior. This is true regardless which scenario period is considered. This reflects the identifiability problem mentioned above, and indicates that the likelihood of the data has only a minor impact on the width of the posterior distribution. This is also evident from *Figure 7*(b), where the posterior uncertainty of $\Delta\mu$ is plotted as a function of $\sigma^2_{\Delta\beta}$ for the three different scenario periods and all four seasons. The uncertainty of $\Delta\mu$ does only marginally depend on the season and time interval considered. Yet, the uncertainty range is to a large degree affected by the number of participating models. As shown in *Figure 7*(c), a reduction of the model sample size from eight models down to two (arbitrarily chosen) models systematically increases the uncertainty in $\Delta\mu$ at each prior setting of $\sigma^2_{\Delta\beta}$. These findings are hardly affected by the choice of models (not shown). Overall, *Figure 7* shows that the posterior uncertainty of $\Delta\mu$ is directly linked to the (ultimately subjective) prior setting of $\sigma^2_{\Delta\beta}$ and the number of models available, while the likelihood (i.e. the actual data values) are only of minor importance. This result is consistent with the sensitivity analysis conducted by Buser *et al.* (2009, Figure 11). Within the current study, it motivates further considerations when defining the hyper-parameter $\sigma^2_{\Delta\beta}$.

In Buser *et al.* (2009), the hyper-parameter $\sigma^2_{\Delta\beta}$ for temperature was set to a fixed value of 0.5 K^2, corresponding to allowed projections in the range −1.4 to

Table II. Hyper-parameters for the prior distributions of (square root transformed) precipitation.

Parameter	Expectation value μ_0 (in $\sqrt{mm/month}$)	Variance σ_0^2 (in *mm/month*)	95% Confidence interval (in $\sqrt{mm/month}$)
μ (for all seasons)	10	25	[0.2, 19.8]
$\Delta\mu$	0	25	[−9.8, 9.8]
β_i	0	25	[−9.8, 9.8]

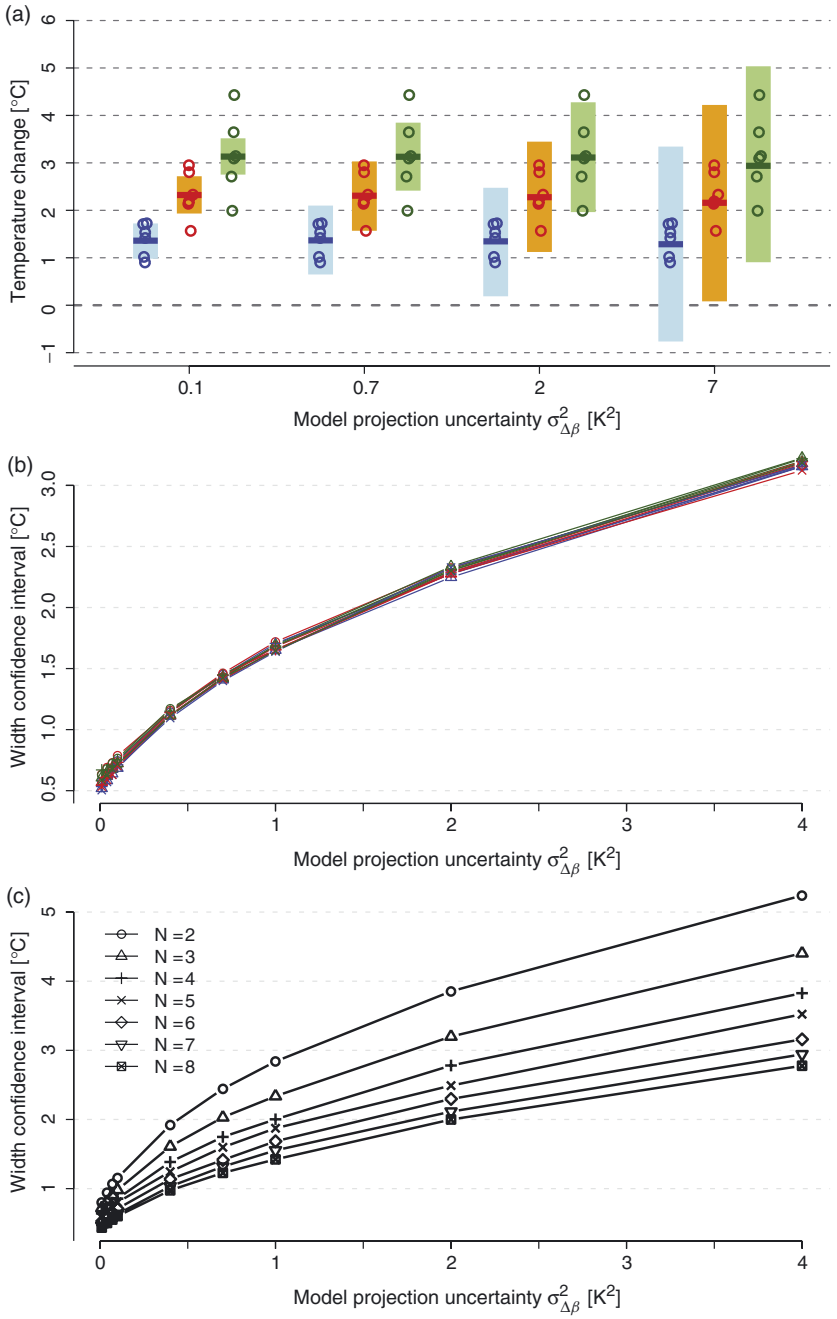

Figure 7. Uncertainty in the posteriori distribution of the climate change parameter ($\Delta\mu$) as a function of the prior choice of model projection uncertainty (variance $\sigma^2_{\Delta\beta}$) for temperature over CHNE. In (a) winter changes for three scenario periods (blue: 2035, red: 2060, green: 2085) are shown. The bars indicate the 95% confidence interval of $\Delta\mu$ with the median as bold horizontal line, while the coloured circles are the raw model output (averaged according to the driving GCM). (b) Width of 95 % confidence intervals of $\Delta\mu$ as a function of $\sigma^2_{\Delta\beta}$ for the three scenario periods (colours are as in panel a) and four seasons (DJF: circle, MAM: triangle, JJA: plus, SON: cross). (c) Width of 95% confidence intervals of $\Delta\mu$ as a function of $\sigma^2_{\Delta\beta}$ for summer and for scenario period 2035 with a varying number of arbitrarily selected models (from $N = 2$ models to $N = 8$ models) used in the BAB.

+1.4K (95% confidence interval). As a justification, it was argued that the model projection errors should be comparable or smaller than typical biases in the control period (note that their analysis was based on PRUDENCE RCM simulations with smaller biases than the ENSEMBLES model runs used here, see Section 2.3.). However, as has been illustrated by the experiments above, applying one fixed (and more or less arbitrary) prior value of $\sigma^2_{\Delta\beta}$ leads to relatively similar posterior uncertainty estimates of $\Delta\mu$, regardless which region, season and lead time is considered. This is inconsistent with the fact that the raw projections reveal an inter-model spread and, thus, projection uncertainties which (1) usually increase with lead time, and (2) may vary significantly from season to season and region to region. To circumvent this obvious inconsistency, we apply the more flexible prior assumption that model error uncertainty is fully sampled by the available model runs. As will be outlined below,

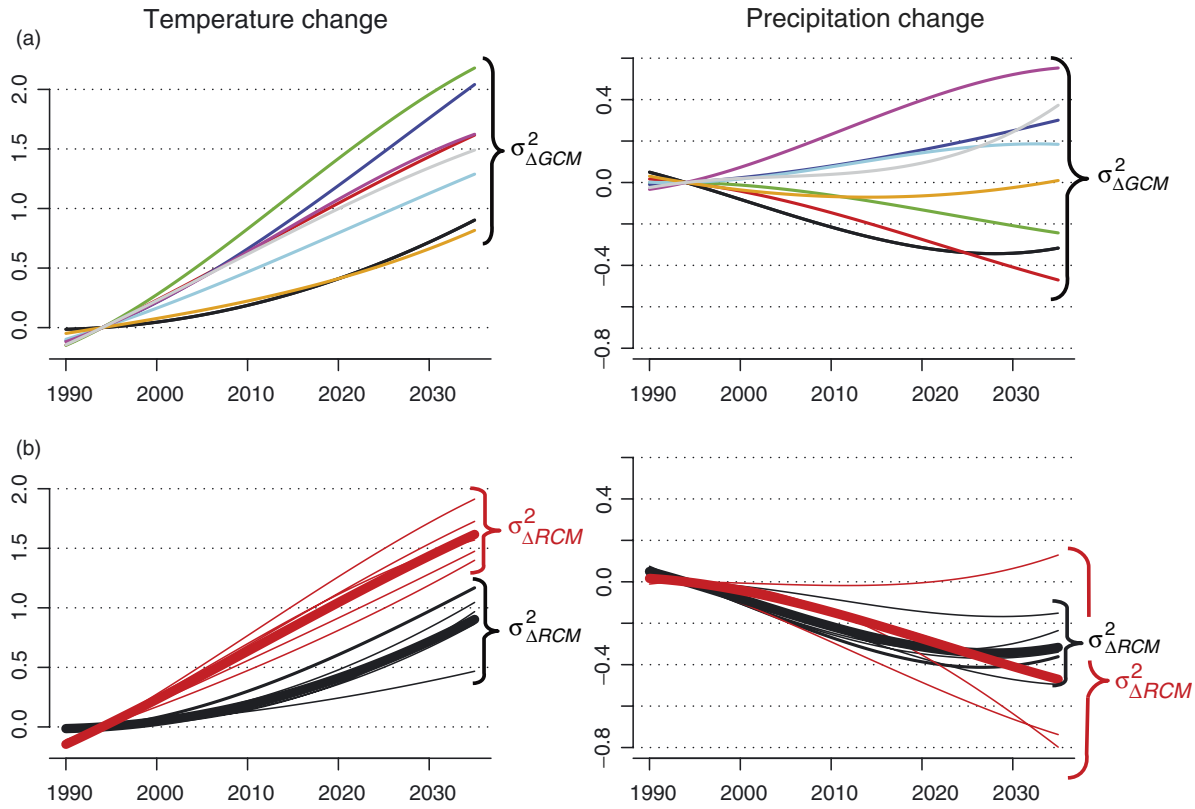

Figure 8. 4th-order polynomial fits (with respect to the central year of 1980–2009) of winter temperature (left, in °C) and summer precipitation (right, in $\sqrt{mm/month}$) over CHNE: (a) Time series averaged according to the driving GCM (different colours indicate a different GCM). The inter-model variance at a scenario-period of interest (illustrated by the brackets) is used as a prior estimate for GCM-uncertainty $\sigma^2_{\Delta GCM}$. (b) Time series of RCM simulations driven by ECHAM5 (black) and HadCM3Q0 (red). The bold line is the corresponding RCM-average. The average of the intra-GCM variances (illustrated by the brackets) is used as a prior for RCM-uncertainty $\sigma^2_{\Delta RCM}$.

this assumption allows applying individual values of the hyper-parameter $\sigma^2_{\Delta\beta}$ for each projection context, i.e. for each combination of lead time, season, region, and variable. Of course, this assumption is still subjective and there are arguments against it. For instance, it ignores the fact that climate models may share similar structural assumptions and the same 'unknown unknowns' in terms of our physical process understanding which can lead to correlated errors (e.g. Jun *et al.*, 2008). However, since with the data and methods at hand it is not possible to quantify the uncertainty of these 'unknown unknowns', we will stick to this assumption for lack of better alternatives, and we stress that the posterior projection uncertainties obtained can only be considered as lower estimates of the true model uncertainty ranges.

To determine prior values of $\sigma^2_{\Delta\beta}$, we assume that it can be decomposed into two components: one characterizing the uncertainty originating from the large-scale driving fields of the GCMs ('GCM uncertainty' $\sigma^2_{\Delta GCM}$), and the other characterizing the uncertainty of limited-area models that translate the large-scale projections onto a localized scale ('RCM uncertainty' $\sigma^2_{\Delta RCM}$). This decomposition is motivated by the fact that the number of RCMs per driving GCM is highly variable (from 5 RCMs driven by 1 GCM down to 1 RCM only, shown in *Figure 1*), so that the model projections applied in the BAB, $\hat{X}^{(3)}_{i,t}$), are affected by both GCM uncertainty and RCM uncertainty.

To estimate GCM uncertainty, the divergence of the model projections, averaged according to driving GCM (i.e. $\hat{X}^{(3)}_{i,t}$), is analysed. To exclude natural fluctuations, only the smooth fourth-order polynomial fits (Section 3.1.1.) through $\hat{X}^{(3)}_{i,t}$ are considered for the analysis. Since we are interested in the model divergence that has built up with respect to the reference period, the smooth fits obtained are shifted such that they overlap in 1995, i.e. the centre of the reference period. This is illustrated in *Figure 8*(a). For a given parameter, region, season, and lead time, $\sigma^2_{\Delta GCM}$ is then estimated by the corresponding inter-model variance at the centre of the scenario period of interest (2035 in the example of *Figure 8*(a)).

To assess RCM uncertainty, $\sigma^2_{\Delta RCM}$, the average 'intra-GCM' spread is considered. That is, for each driving GCM, the spread of the RCM time series $\hat{X}^{(2)}_{m,t}$ driven by this GCM is evaluated, and the average of these spread values is used as an estimate for $\sigma^2_{\Delta RCM}$. Again, the time series are smoothed by a polynomial fit and evaluated with respect to a common reference in 1995. This is illustrated in *Figure 8*(b) for the RCMs driven by 2 GCMs. Of course, this approach requires that a sufficient number of RCMs (at least 5) is available that have been driven by the same GCM. For the ENSEMBLES models, this is only the case for ECHAM5 and HadCM3Q0

Table III. Hyper-parameters estimated for model projection uncertainty (hyper-parameter $\sigma^2_{\Delta\beta}$) in temperature (in K^2) and (square root transformed) precipitation (in *mm/month*) according to region, scenario period and season. The numbers in italic indicate the fraction of $\sigma^2_{\Delta\beta}$ (in %) explained by GCM uncertainty and by RCM uncertainty. Note that for 2060 and 2085 the estimates are based on 14 instead of 20 RCM-GCM chains with a reduced number of GCMs (see text).

		CHNE						CHW						CHS					
		2035		2060		2085		2035		2060		2085		2035		2060		2085	
		GCM	*RCM*	*GCM*	*RCM*	*GCM*	*RCM*	*GCM*	*RCM*	*GCM*	*RCM*	*GCM*	*RCM*	*GCM*	*RCM*	*GCM*	*RCM*	*GCM*	*RCM*
Temperature	**DJF**	0.28		0.48		0.89		0.27		0.44		0.83		0.32		0.77		1.46	
		83	*17*	*79*	*21*	*84*	*16*	*78*	*22*	*81*	*19*	*87*	*13*	*78*	*22*	*86*	*14*	*79*	*21*
	MAM	0.54		0.68		1.04		0.47		0.67		1.03		0.58		0.63		0.90	
		96	*4*	*99*	*1*	*98*	*2*	*93*	*7*	*97*	*3*	*97*	*3*	*93*	*7*	*95*	*5*	*97*	*3*
	JJA	0.39		0.65		1.57		0.42		0.75		1.69		0.44		0.84		1.81	
		93	*7*	*94*	*6*	*83*	*17*	*88*	*12*	*95*	*5*	*84*	*16*	*78*	*22*	*93*	*7*	*84*	*16*
	SON	0.43		0.95		1.82		0.44		1.02		1.90		0.43		0.88		1.69	
		92	*8*	*98*	*2*	*99*	*1*	*92*	*8*	*98*	*2*	*98*	*2*	*90*	*10*	*97*	*3*	*96*	*4*
Precipitation	**DJF**	0.46		0.14		0.12		0.46		0.12		0.12		0.21		0.40		0.51	
		77	*23*	*95*	*5*	*88*	*12*	*67*	*33*	*96*	*4*	*88*	*12*	*42*	*58*	*94*	*6*	*90*	*10*
	MAM	0.12		0.12		0.25		0.12		0.05		0.17		0.26		0.13		0.19	
		47	*53*	*88*	*12*	*92*	*8*	*53*	*47*	*90*	*10*	*95*	*5*	*75*	*25*	*42*	*58*	*58*	*42*
	JJA	0.19		0.12		0.35		0.16		0.08		0.27		0.25		0.10		0.39	
		67	*33*	*53*	*47*	*55*	*45*	*62*	*38*	*51*	*49*	*69*	*31*	*29*	*71*	*70*	*30*	*55*	*45*
	SON	0.19		0.29		0.46		0.17		0.23		0.36		0.22		0.37		0.81	
		77	*23*	*93*	*7*	*87*	*13*	*70*	*30*	*93*	*7*	*90*	*10*	*54*	*46*	*86*	*14*	*93*	*7*

driven runs if lead times up to 2050 are considered. Even worse, for lead times beyond 2050 it is only ECHAM5 which has driven enough RCMs. Hence, in this study, for the 2035 projections $\sigma^2_{\Delta RCM}$ is estimated by the average between the intra-ECHAM5 variance and the intra-HadCM3Q0 variance (*Figure 8*(b)), while for the 2060 and 2085 projections only the intra-ECHAM5 variance is used.

With this, the prior of total model projection uncertainty can be obtained by summing up the two uncertainty components

$$\sigma^2_{\Delta\beta} = \sigma^2_{\Delta GCM} + \sigma^2_{\Delta RCM} \quad \textbf{(9)}$$

Table III. provides a detailed overview of the $\sigma^2_{\Delta\beta}$ estimates for each parameter, scenario period, region, and season. Additionally, the table shows, in italics, the relative contributions of GCM and RCM uncertainty to the estimates of $\sigma^2_{\Delta\beta}$. For temperature, in general, the $\sigma^2_{\Delta\beta}$ estimates obtained increase with lead time, and in most cases they exceed the value of 0.5 proposed by Buser *et al*. (2009) already for scenario period 2060. The largest $\sigma^2_{\Delta\beta}$ values are seen for JJA and SON at the end of the century, with estimates being about 4–5 times larger than for 2035. Inter-regional differences in the estimates are relatively small. One exception is CHS in winter during the second half of the century, where model deviations are much higher than for CHNE and CHW. In general, for temperature, the variability across the GCMs, i.e. $\sigma^2_{\Delta GCM}$, is the dominating contributor to model projection uncertainty. This is qualitatively in line with the findings of Déqué *et al*. (2007), which were based on data from the PRUDENCE project. During DJF and JJA, the RCMs explain at most up to 22% of the total model projection uncertainty, while for MAM and SON the fraction is usually less than 10%.

For precipitation, the prior estimates of projection uncertainty are also generally largest at the end of the century. However, the increase is less continuous and shows higher dependency on region and season than temperature. In many cases, the $\sigma^2_{\Delta\beta}$ estimates for 2035 are as high as, or even higher than for the 2060 scenarios. This is most evident for winter over CHNE and CHW, where the variance estimates for the 2035 projections are almost 4 times larger than for the 2060 and 2085 scenarios. These differences are partly due to sampling uncertainty arising from the small number of model chains available, particularly for the second half of the 21st century. As will be discussed later, seasonal mean precipitation in Switzerland is (in contrast to temperature) only moderately affected by global warming and associated with low signal-to-noise ratios. In consequence also, the underlying model uncertainty is only moderately dependent on the lead time, and hence, estimates of model uncertainty are likely dominated by sampling uncertainty. Apart from that, the differences in variance might also be an indication that a 30-year moving average time window is not wide enough to fully remove natural variability from precipitation.

For precipitation, the contribution of the RCM component to projection uncertainty is, at least for 2035, with values between 23 and 71% much larger than in case of temperature. Especially for summer, the choice of RCM remains a large source of uncertainty also until the end of the century (between around 30 and 45%). This is again consistent with the analyses of Déqué *et al*. (2007).

3.3. Post-processing of the posterior distribution

Through the application of all methodological steps so far explained (Section 3.1.–3.2.), we derive posterior distributions of all parameters specified in Equation (7). For

the climate scenarios presented in this study, it is particularly the posterior distribution of climate mean shift ($\Delta\mu$) which is of central interest. However, two further post-processing steps are required. Firstly, for precipitation, it is common practice to formulate climate projections of precipitation in terms of relative precipitation change. This requires an appropriate transformation of $\Delta\mu$, since $\Delta\mu$ represents the square root of absolute precipitation change (Section 3.1.2.). Secondly, internal decadal variability is not yet included in the uncertainty estimates and therefore needs to be re-added. These two steps are explained more in detail in what follows.

3.3.1. Re-transformation of precipitation posterior densities

As mentioned above, $\Delta\mu$ represents the expected change of root-mean-transformed precipitation values. Owing to the nonlinearity of the square root operator, the change of absolute precipitation cannot be expressed by simply squaring $\Delta\mu$. Rather, the square operator needs to be applied on the posterior estimate of total square root precipitation, $\mu + \Delta\mu$, with μ being the posterior estimate of mean square root precipitation during the reference period. The projected change of absolute precipitation is then given by the difference $(\mu + \Delta\mu)^2 - \mu^2$, and the expected change of relative precipitation (which will be used in the next sections) becomes

$$\Delta\mu^{NEW} = \frac{(\mu + \Delta\mu)^2 - \mu^2}{\mu^2} \qquad \textbf{(10)}$$

Note that the nonlinear re-transformation affects not only the central tendency, but also the variance of the posterior outcome in a nonlinear way.

3.3.2. Recombination of internal variability

As discussed in Section 3.1.1., the BAB has required internal decadal variability (i.e. $< \varepsilon_{0,t} >_{30yr}$ and $< \varepsilon_{m,t} >_{30yr}$) to be removed prior to model combination. For the final probabilistic temperature and precipitation scenarios, this subtracted variability contribution needs to be recombined with the posterior distribution of $\Delta\mu$. This is technically done by summating the individual samples of $\Delta\mu$ as obtained from the Gibbs sampler in the BAB with randomly sampled values of observed internal decadal variability ($< \varepsilon_{0,t} >_{30yr}$) to yield the new re-combined mean change ($\Delta\mu^{Mod+IV}$):

$$\begin{aligned} \Delta\mu^{Mod+IV} &= \Delta\mu + < \varepsilon_{0,t} >_{30yr} \\ with \; &< \varepsilon_{0,t} >_{30yr} \sim \mathcal{N}(0, 2\sigma_{IV}^2) \end{aligned} \qquad \textbf{(11)}$$

Since $\Delta\mu$ describes the difference between 'observations' expected for the future and observations made during the control period, internal variability needs to be added twice, i.e. the simulated values of internal decadal variability are generated using twice the variance estimate of observed variability (i.e. $2\sigma_{IV}^2$). To obtain more robust estimates of observed internal variability, σ_{IV}^2 has been estimated from historical homogenized surface measurements of MeteoSwiss, ranging back to 1864 (Begert *et al.* 2005), rather than from E-OBS data which are available only back to 1950. The methodology is as described in Section 3.1.1. First, a smooth 4th-order polynomial is fit to the observational time series from 1864 to 2009, and in a second step the 30-year mean residuals from this smooth fit are calculated. σ_{IV}^2 is given by the variance of these residuals. In this study, station data at Basel and Zurich are used to estimate σ_{IV}^2 for CHNE; the stations at Geneva and Berne are used for CHW, and the station at Lugano for CHS.

3.4. Estimating changes for other emission scenarios

Climate change projections are conditioned on assumptions how global emissions of greenhouse gases and aerosols as well as land use changes evolve in the future. The choice of emission scenario significantly affects the magnitude of climate change especially towards the end of the century (IPCC, 2007). Since the ENSEMBLES RCM model chains are all conditioned on the A1B emission scenario, the sensitivity of the projections to different emission assumptions cannot be explored on the basis of RCM data alone. To overcome this deficiency, a pattern-scaling approach has been applied (Santer *et al.*, 1990; Mitchell, 2003; Fowler *et al.*, 2007). This method, as used here, is based on the assumption that regional temperature and precipitation changes can be approximated by multiplying a spatially invariant change pattern, normalized to a one degree global temperature change, with the global mean temperature change of any emission scenario as obtained from GCMs or energy balance models (EBMs).

We use this technique to scale the projections obtained from the A1B ENSEMBLES runs to two other scenarios: a non-intervention scenario with high fossil fuel emissions (A2; Nakicenovic and Swart, 2000), and a strong carbon mitigation scenario which likely prevents global warming of more than 2 °C with respect to the pre-industrial period (RCP3PD, van Vuuren *et al.*, 2007). Since we assume that internal variability is not affected by the choice of emission scenario, the scaling must be applied prior to re-adding internal variability (Section 3.3.2.).

Starting from climate change projections obtained for the A1B emission scenario, $\Delta\mu^{A1B}$, the pattern-scaled estimates of the projections for the A2 and RCP3PD scenarios are obtained with the following equation:

$$\Delta\mu^{[A2,RCP3PD]} = \frac{< \Delta T2_{global}^{[A2,RCP3PD]} >}{< \Delta T2_{global}^{A1B} >} \cdot \Delta\mu^{A1B} \qquad \textbf{(12)}$$

Here, the magnitude of global warming ($\Delta T2_{global}$) to be expected for the A1B and A2 emission scenarios are estimated from the multi-model mean of coupled GCMs (IPCC, 2007), while that to be expected for the RCP3PD emission scenario are estimated from the reduced complexity coupled climate-carbon cycle model MAGICC (Meinshausen *et al.*, 2009). The scaling factors

Table IV. Pattern-scaling factors (based on global temperature) applied to probabilistic ENSEMBLES projections (A1B scenario) to estimate probabilistic scenarios for the A2 and RCP3PD emission scenario for the three target periods.

	2035	2060	2085
A2	0.89	0.98	1.17
RCP3PD	0.95	0.60	0.43

obtained for the A2 and RCP3PD emission scenarios for the three periods considered are listed in Table IV. In comparison to the A1B scenario, a future world according to the A2 scenario would imply a global warming that is enhanced by 17% in 2085. On the other hand, by 2035, the warming is reduced by around 10% compared to the A1B scenario. The reason for these scaling factors with opposing signs lies in the global emission pathways of the A2 and A1B scenario over the 21st century (Nakicenovic and Swart, 2000). The mitigation scenario RCP3PD leads to a stabilisation of global mean temperature rises such that the warming by 2060 (2085) is around 40% (57%) lower than in case of the A1B scenario.

Although pattern scaling is a widely used technique in climate and impact studies (e.g. Jenkins *et al*., 2009), it is important to stress that it comes with several limitations (Mitchell, 2003). By definition, the method is only valid as long as the response linearly scales with global mean temperature. For spatial scales such as analysed here, this might not always be the case due to a number of nonlinearities induced by feedback processes or threshold effects (e.g. associated with soil moisture or snow dynamics). The applicability is further questionable when linearly scaling precipitation changes from a non-mitigation scenario to an aggressive mitigation scenario (Wu *et al*., 2010). Yet, for the lack of a better alternative, pattern scaling still remains the best available method at hand.

For the purpose of the present study, we evaluated the pattern scaling method by scaling the A1B posterior distribution of $\Delta\mu$ from one scenario period to another (i.e. scaling $\Delta\mu$ at 2085 toward 2035). The comparison of the scaled projections with the actual probabilistic estimates as obtained with the BAB has revealed that the pattern-scaling approach works reasonably well for both temperature and precipitation. In general, differences between the scaled projections and the BAB estimates are small. The largest discrepancies of the median changes are seen during the summer season and amount to about 0.2 K for temperature and 6% for precipitation. This is likely due to nonlinear responses in the regional climate over the 21st century during this season. However, these differences are small in comparison to the other uncertainties present in the climate scenario cascade.

4. Results: Temperature and precipitation scenarios over Switzerland

The resulting probabilistic scenarios for seasonal temperature and precipitation changes over the 21st century are displayed in Figure 9 and 10. The uncertainty ranges are shown, expressed as 95% confidence intervals (coloured bars), together with the median estimate (bold horizontal line) for the 3 emission scenarios and the 3 regions. The underlying model projections are superimposed onto the bars of the A1B scenario. This is raw model output, averaged according to the driving GCM, and including internal decadal variability. Note again that each of the individual confidence intervals results from a separate calculation applying the methodological steps discussed in Section 3.

4.1. Probabilistic temperature projections

The probabilistic projections show that temperature changes in Switzerland are positive for all seasons, regions, and emission scenarios analysed. For the A1B and A2 emission scenarios, the warming signal increases with lead time, while the projected temperature changes of the RCP3PD scenario stabilize in the second half of the century.

For the A1B emission scenario, depending on region and season, the median estimates indicate a warming of 0.9–1.4 °C by 2035 that further increases by about 1 °C (by about 2 °C) by 2060 (by 2085). In summer, however, this increase is considerably stronger (up to 1.5 °C by 2060) than during the other seasons, so that seasonal differences in the warming signal become more evident towards the end of the century. By then, also interregional differences, such as a more pronounced warming over CHS compared to north of the Alps, become apparent. For example, by 2085, the median estimates for CHS indicate a warming of 3.3 °C (DJF), 3.1 °C (MAM), 4.1 °C (JJA) and 3.2 °C (SON), while for the two regions north of the Alps this amounts to around 3.1 °C (DJF), 2.8 °C (MAM), 3.8 °C (JJA), and 3.2 °C (SON). So overall, the range of warming (median estimates) across the different regions and seasons for the A1B scenario is on the range of 0.9–1.4 °C by 2035, 2.0–2.9 °C by 2060, and 2.7–4.1 °C by 2085 (all relative to 1980–2009).

Up to 2035, the choice of the emission scenario has only a weak impact on the projected changes. However, for longer projection times, the different scenarios increasingly diverge. By 2085, the impact of the emission scenario on the projected temperature change is to the order of several degrees. For instance, while the median estimates of temperature increase for the A2 emission scenario are within the range of 3.2–4.8 °C (depending on region and season considered), the projected temperature change of the RCP3PD scenario is around 1.2–1.8 °C.

The uncertainty range in temperature changes generally increases with lead time for the A1B scenario. This was to be expected, as it reflects the increasing divergence of model projections over the century and, hence, our prior estimates of $\sigma^2_{\Delta\beta}$ (Table III), which largely determine the uncertainty in the climate change signal (Section 3.2.2.). However, due to the recombination of internal decadal variability with the posterior distribution (Section 3.3.2.), the relative magnitudes of the $\sigma^2_{\Delta\beta}$ estimates

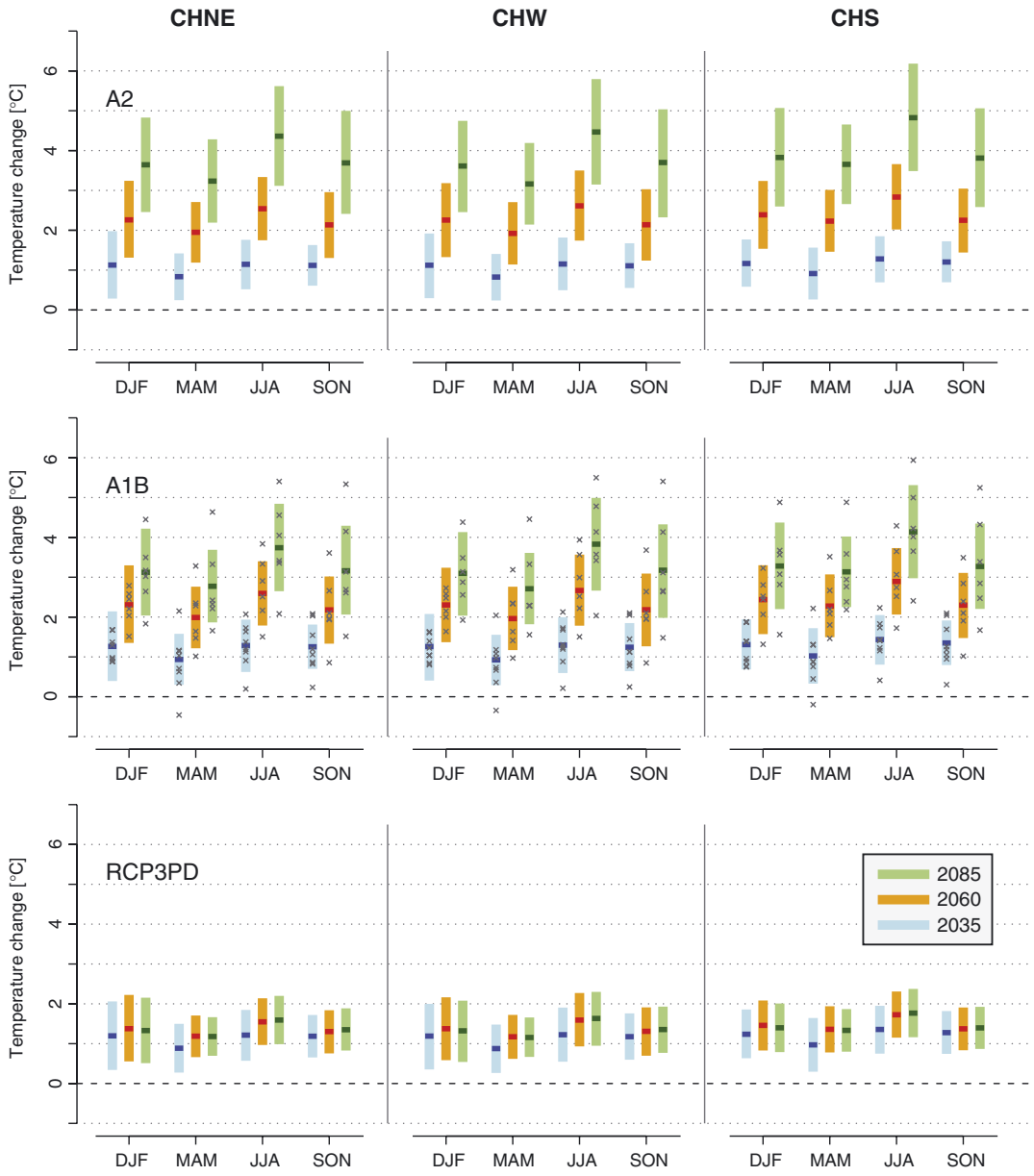

Figure 9. Probabilistic temperature change scenarios (in °C) according to emission scenarios (row) and regions (columns). The coloured bars represent the 95% confidence interval in the climate shift parameter (including internal decadal variability) with the median as bold horizontal line. The crosses in the middle row are the raw model projections (averaged according to driving GCM and including internal decadal variability).

across different regions, seasons and lead times may differ from the relative magnitudes of uncertainty ranges in the probabilistic scenarios.

For the A1B scenario, by 2085, the lower end of the uncertainty bars amounts to 1.8–3.0 °C warming (across all regions and seasons) and the upper end to 3.6–5.3 °C. Note that some individual model projections lie well outside the uncertainty bars. This indicates that the BAB considers them to be unlikely. Whether or not a model is treated as an outlier is solely based on the likelihood (Equation (7)), on the magnitude of decadal variability, and on our prior assumptions (in particular $\sigma^2_{\Delta\beta}$, Figure 7). This is, for instance, the case for two model projections, with one significantly above and one below the majority of models in 2060 and 2085. Also note that an outlier such as the model projection that suggests a cooling by 2035 in spring over CHNE and CHW is considered unlikely, given the other 7 positive temperature model projections. A similar effect had already been observed by Buser *et al.* (2009).

The choice of emission scenario not only affects the mean estimate but also the uncertainty range that, in case of the A2 scenario, by the end of the century is substantially larger than in the first half of the century. In case of the RCP3PD scenario, the uncertainty ranges in the second half of the century are similar to those by 2035, but somewhat reduced in spring north of the Alps.

4.2. Probabilistic precipitation projections

The uncertainty ranges of regional precipitation projections for Switzerland are generally large. In fact, in winter, spring, and autumn, even the sign of the change signal

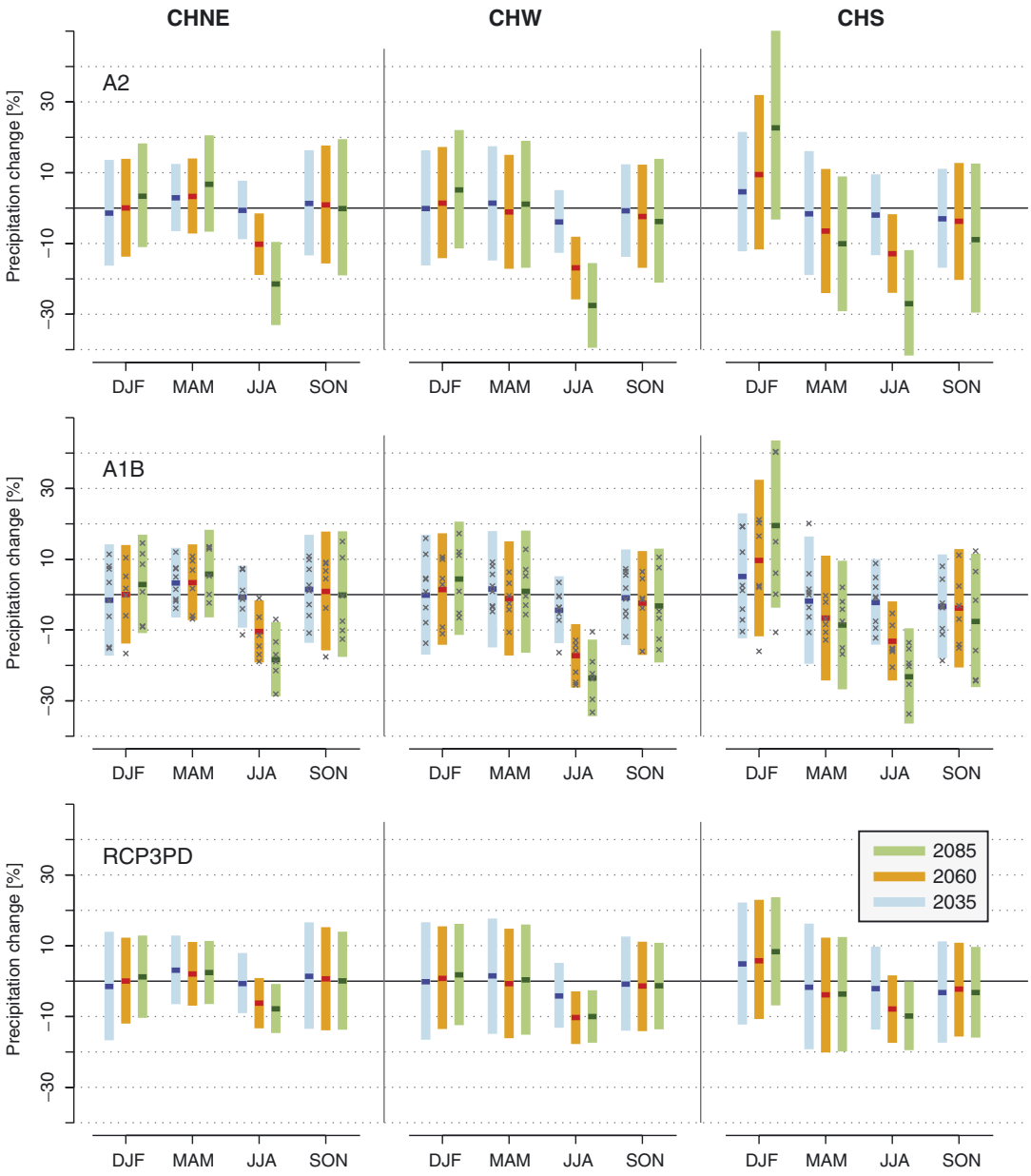

Figure 10. As in Figure 9, but for precipitation changes (in %).

can either be positive or negative and remains uncertain in all of the analysed regions and emission scenarios (Figure 10). The exception is summer when a significant decrease in precipitation in the second half of the century is expected for A2 and A1B over all regions and for RCP3PD over CHW.

For the A1B scenario, this decrease amounts to 10–17% by 2060, and 18–24% by 2085, with the change signal being strongest over CHW. Moreover, south of the Alps, there is an indication of an upward trend in winter precipitation in the course of the century. By 2085, the median estimates lie at +20%, but negative changes cannot be ruled out. Apart from that, the median precipitation changes are generally close to zero with an uncertainty range of 20–40% covering both an increase and decrease. The probabilistic scenarios obtained with the BAB seem to be fully consistent with the individual projections of the model set: whenever the uncertainty bars indicate that changes in both directions are possible, there is at least one model with zero or an opposite change signal compared to the rest of the models. Another example of consistency is the very large uncertainty bar for CHS in winter by 2085, which can be explained by the fact that 2 (out of 6) models exhibit a precipitation change of around +40% and are hence regarded as plausible outcome by the BAB.

In general, for the A1B and A2 scenario, the uncertainty range increases with lead time. However, the increase is less apparent than it is for temperature. For winter over CHW and CHNE, between the scenario periods 2035 and 2060, uncertainty even decreases. This reflects to some degree the behaviour of prior estimates of $\sigma^2_{\Delta\beta}$ in Table III (much higher value in 2035 than in 2060). As for temperature, internal variability has in

many cases a significant impact on the projection uncertainty as well.

Differences due to the choice of emission scenario become especially evident towards the end of the century. For instance, in 2035, summer precipitation over CHW varies by less than 1% across the three different scenarios, while by 2085, the projections range from a decrease of 10% for the RCP3PD scenario to a decrease of 28% for the A2 scenario.

5. Discussion

The probabilistic scenarios presented in Section 4 provide an essential update on climate change information over Switzerland making use of the latest set of highly resolved model simulations over Europe and using a state-of-the-art multi-model combination algorithm. While the temperature projections show a pronounced warming signal with a magnitude that is consistent with earlier projections for Switzerland (Frei, 2004; OcCC, 2007), the projections of precipitation do not reveal a clear tendency in terms of the expected sign of change for all seasons except summer where a drying is projected. Any precipitation change signal that may exist for spring, autumn, and winter appears to be shadowed by the large uncertainty ranges that are generally larger for precipitation than for temperature (Hawkins and Sutton, 2009, 2011). In fact, even on a global scale there are still considerable uncertainties concerning past and future changes in the water cycle (e.g. Allan and Soden, 2007; Zhang *et al*., 2007). Moreover, two further factors are responsible for the lack of signal in precipitation: the large magnitude of internal variability (not shown) and the geographic location of Switzerland at the transition zone between two larger-scale patterns of precipitation change. To better understand these large-scale processes, we proceed with a short analysis of the patterns of temperature and precipitation change over Europe.

Figure 11 displays the projected temperature changes under the A1B emission scenario. Shown is the multi-model mean (RCMs have been averaged according to driving GCM prior to determining the multi-model mean) which indicates a large-scale warming pattern over Europe across the 21st century. The strongest increase is projected for northern Europe in winter and southern Europe in summer. Consistent with this pan-European warming, Switzerland will experience a continuous rise in temperature that is amplified with lead-time (see also *Figure 9*). In contrast to temperature, the large-scale relative precipitation changes over Europe (*Figure 12*) are characterized by a pronounced north-south contrast that grows with lead time: precipitation is projected to increase in northern Europe and to decrease in southern Europe. This large-scale change pattern can be explained both by circulation changes and thermodynamic factors (Rowell and Jones, 2006; van Ulden and van Oldenborgh, 2006). While the changes are still moderate by 2035, the bipolar structure of the change pattern intensifies towards the end of the century. The location of the transition zone separating the northern European precipitation increase and the southern European precipitation decrease reveals a pronounced seasonal cycle, shifting northwards in summer and southwards in winter. In summer, the transition zone is in northern Europe, so that Switzerland is located well within the large-scale pattern of southern European drying. In fact, the largest changes are to be expected for the region west of Switzerland (France and the northern Iberian Peninsula). This intensification towards the west is reflected in the drying signal over Switzerland, which is stronger over CHW than over CHNE and CHS (Figure 10). During the other seasons (spring, autumn, winter), Switzerland and much of Central Europe is located at or near the transition zone, implying that the projected precipitation changes for Switzerland are comparatively small, or at least uncertain, for these seasons. This essentially explains why neither the mean projections nor the model uncertainties reveal a pronounced signal, and why the projections are almost independent from lead time.

6. Summary and conclusion

The purpose of this study has been to illustrate how a recently developed Bayesian methodology can be applied to RCM output to obtain regional probabilistic projections of temperature and precipitation change in response to given greenhouse gas scenarios. This has been done on the basis of the Bayesian multi-model combination algorithm of Buser *et al*. (2009), BAB, illustrated for the case of Switzerland. The scenarios are based on the ENSEMBLES RCM projections and have been calculated for three regions, four seasons, three lead times, and three emission scenarios. The applicability of the algorithm for the projection context discussed in this study involves several major conceptual and methodological challenges:

Firstly, how can internal decadal variability be accounted for, given that the BAB, by construction, assumes that discrepancies between different model projections are exclusively due to model uncertainty? We have shown that this problem can be circumvented by filtering out internal decadal variability from the observational and model time series prior to the model combination and re-adding it to the posterior distribution of the climate change signal after model combination.

Secondly, how can quantitative estimates be obtained for different emission scenarios (here A1B, A2, RCP3PD), given that a sufficient number of ENSEMBLES RCMs are only available for the A1B emission scenario? This has been done by the technique of pattern scaling, which has been applied to the posterior distributions of the climate change signals prior to recombination with internal variability. By doing so, it has been assumed that internal decadal variability is independent of global mean temperature changes.

Thirdly, how can correlated model errors be minimized (the BAB requires independence), given that several

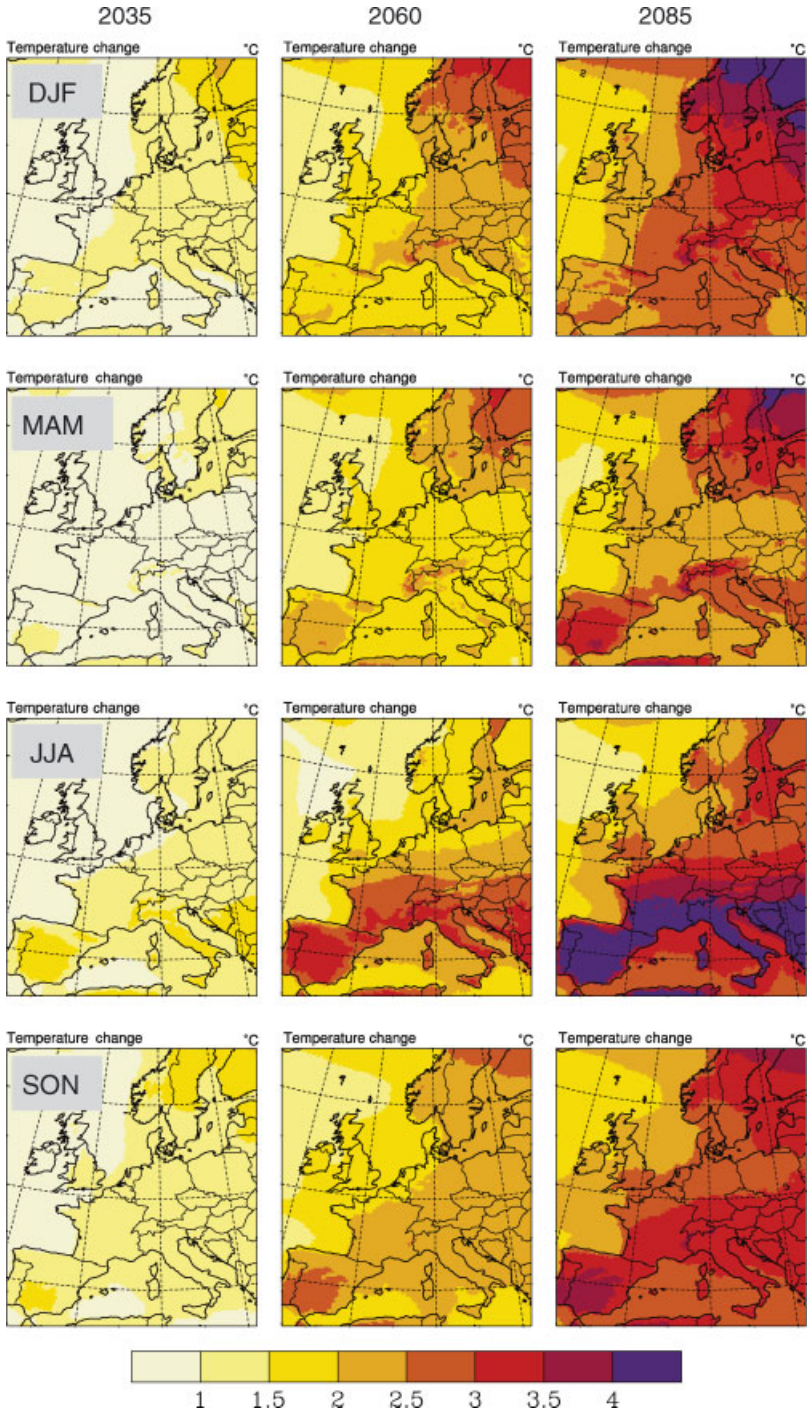

Figure 11. Temperature changes (in °C, relative to 1980–2009) over Europe in the multi-model mean (mean over the projections that were averaged according to the driving GCM beforehand).

RCMs have been driven by the same GCM and therefore reveal pronounced covariances? This requirement has been pragmatically resolved by averaging all RCMs driven by the same GCM, thus reducing the inter-model correlations.

The most difficult challenge has been the choice of a prior assumption on the magnitude of model error uncertainty. We have shown that the choice of this value is directly linked to the posterior projection uncertainty obtained from the BAB and is thus of uttermost importance. In this study, these prior values have been obtained from the assumption that the model runs available fully sample the range of model uncertainty (given below). More specifically, the prior has been assumed to be decomposable into a sum of two variance estimates, one comprising the variability across the different driving GCMs, and one comprising the variability across different RCMs driven by the same GCM.

On the basis of this methodology, and taking 1980–2009 as reference period, probabilistic scenarios of temperature and precipitation changes have been obtained which can be summarized as follows:

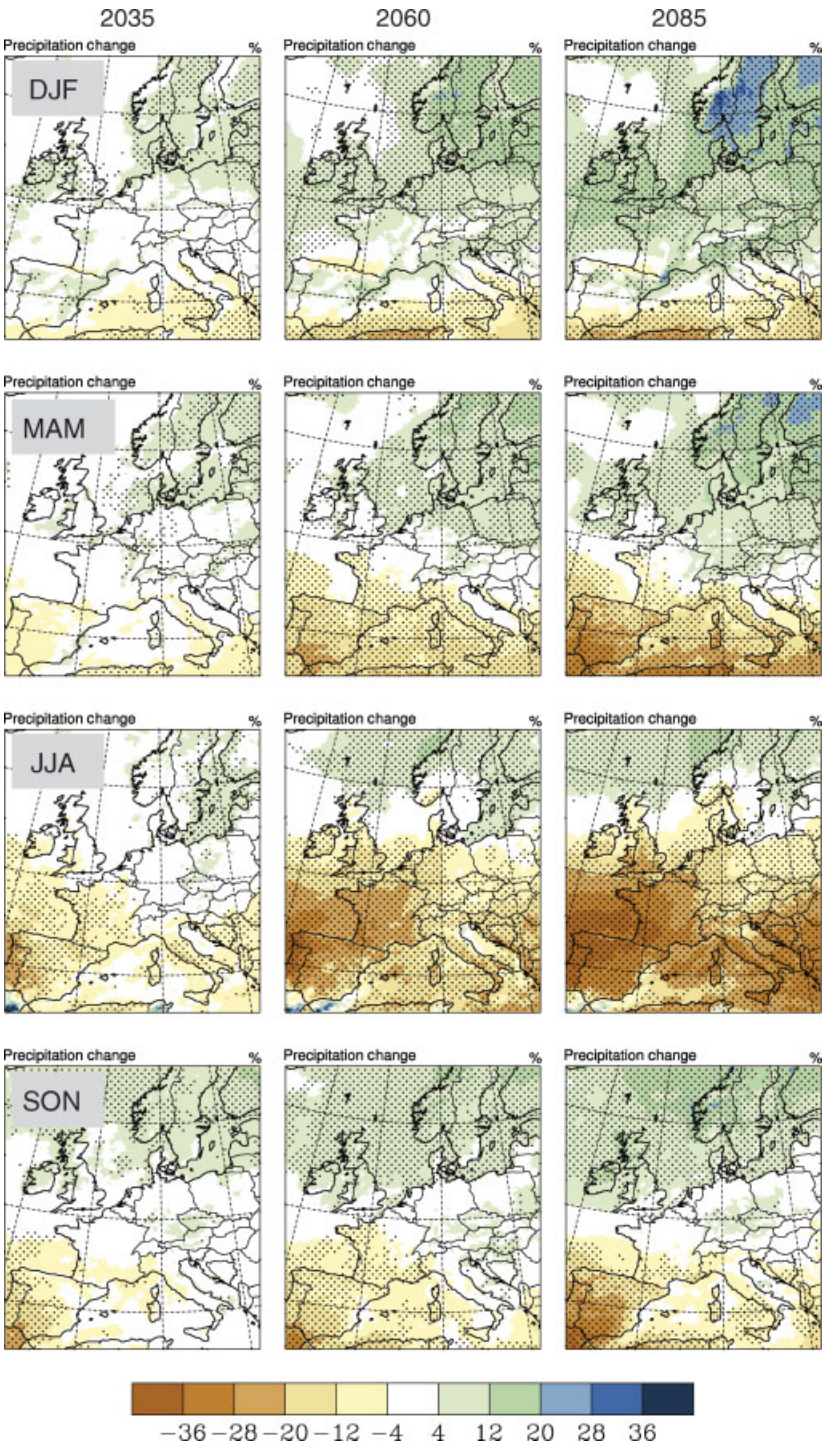

Figure 12. As in Figure 11, but for precipitation changes (in %). The black dots indicate those regions where at least 80% of the models agree on sign.

(1) In the course of the 21st century, Switzerland will experience significant changes in climatic conditions (temperature and precipitation) as compared to the observed climate of the past decades.
(2) The magnitude of climate change in Switzerland depends on region and season, and particularly on the pathway of future greenhouse gas emissions.
(3) If emissions follow a fuel-intensive non-intervention emission scenario (A2), the median estimate indicates (1) an increase of seasonal mean temperature of 3.2–4.8 °C by 2085, depending on region and season, (2) a 21–28% decrease of summer mean precipitation, depending on region, and (3) a 23% increase of winter precipitation south of the Alps.
(4) If effective mitigation measures were implemented to halve greenhouse gas emissions globally by about 50% by 2050 (RCP3PD scenario), climate would still change in Switzerland over the next decades, but is projected to stabilize at 1.2–1.8 °C warming, and an 8–10% summer drying by 2085.

(5) For winter, north of the Alps, and spring and autumn in all of Switzerland, precipitation scenarios do not show a clear tendency for the sign of precipitation change. This is due to the fact that, in these seasons, Switzerland is located at or near the transition zone between two large-scale regimes of precipitation changes: decreases in southern Europe and increases in northern Europe.

It should be emphasized again that probabilistic scenarios, such as those presented and communicated here, are necessarily conditioned on a number of assumptions. Consequently, the projections and uncertainty ranges obtained are only valid to the degree that the underlying assumptions hold or can at least be justified. This applies, for instance, to the estimated projected changes according to the A2 and RCP3PD emission scenarios that are valid only as long as the regional climate response scales linearly with global mean temperature changes over the 21st century (i.e. as long the prerequisites for pattern scaling are satisfied).

On the route to probabilistic scenarios two other fundamental assumptions were made, which we would like to emphasize and revisit here. These are assumptions which in fact are not specific to the methodology applied in the presented study but inherent to many published climate projections.

Assumption 1: The range of model uncertainty is fully sampled by the available model projections.

This is probably the most critical assumption, mainly for the following reasons:

a) The 20 RCM-GCM chains within the ENSEMBLES matrix represent only a subset of all potential RCM-GCM combinations and a subset of all potential GCM projections currently in use worldwide (IPCC, 2007). This is even aggravated in the second half of the century with the reduced ENSEMBLES set (only six GCMs). It is likely that the model data used in this study only sample a portion of the total model uncertainty, and that the estimates obtained are subject to significant sampling uncertainty. A full exploration of the uncertainty ranges would require (1) a larger ensemble of driving GCMs, and (2) simulations of all possible RCM-GCM combinations so that also the uncertainties stemming from dynamical downscaling can be assessed.
b) All state-of-the-art climate models share similar structural assumptions and the same 'unknown unknowns' in terms of physical process understanding implying correlated error structures (Knutti *et al*., 2010; Masson and Knutti, 2011). The quantification of this so-called structural uncertainty remains an open issue in climate science.
c) Climate models treat many processes and feedbacks only in a simplistic manner. For instance, the still-coarse resolution of the RCMs used in this study does not allow to explicitly resolve convection and associated feedbacks, and the associated uncertainties are known to affect the magnitude and sign of regional climate feedback processes (Hohenegger *et al*., 2009). Other examples are the uncertainties in the carbon cycle climate feedbacks that are not sampled in the present setup because most GCMs are driven with the same atmospheric CO_2 concentrations. Those feedbacks are particularly relevant at the upper end of the climate change distribution (Knutti *et al*., 2008). Moreover, there are indications that climate models in general do not sample the full range of climate sensitivity as estimated from various observational constraints (Knutti and Hegerl, 2008).

Assumption 2: Systematic model biases do not change with time.

This commonly applied (implicit) assumption is the basis of most published climate projections (including IPCC, 2007), and it has also been assumed in the present study. Different bias assumptions may be equally justified. For instance, systematic biases may change with temperature. This may have potentially significant impact on the outcomes (Christensen *et al*., 2008; Buser *et al*., 2009). In particular, for continental Europe, there is some evidence from the aforementioned studies that summer temperature change may be overestimated with the constant bias assumption, while for Scandinavia winter temperature change may be underestimated. However, with the current observational and model data at hand, it is not possible to clearly infer the development of model biases over time. Therefore, the simplest assumption, i.e. the constant bias assumption, has been chosen. It is important to stress, however, that the current Bayesian framework (in distinction to most other climate change studies) actually allows for biases to change, but these changes are minimized (relative to the constant bias assumption) depending upon the prior assumptions. The demonstrated sensitivity thus provides further motivation to investigate other bias assumptions than adopted in the current study.

Both these fundamental assumptions have been made not on the basis of strong scientific arguments, but for lack of suitable alternatives. Given that the scenarios presented here involve a number of further assumptions – as do all published climate projections – and given that they are based on only a small number of GCMs, we ultimately do not recommend to interpret the scenarios obtained in a strictly probabilistic sense. The 2.5 and 97.5% quantiles shown should rather be considered as a lower and upper estimate of pathways of future climate evolution which are consistent with the data and methodology applied, but which may change as more information becomes available and more sources of uncertainty are included. The uncertainties are likely to be bigger than those produced by the BAB for the reasons discussed above.

Whether probabilistic results (e.g. Tebaldi *et al*., 2005; Furrer *et al*., 2007) necessarily have to be presented to the end user in a probabilistic form is another question that is

not simple to answer. Some studies and national assessments have argued for it and have even attempted to also incorporate carbon cycle uncertainties, structural uncertainties, and downscaling uncertainties into a Bayesian framework (e.g. Murphy *et al*., 2007), while others have argued that probabilistic information is not necessarily required for decision making, and in the case of large uncertainties may imply too much accuracy (e.g. Lempert and Schlesinger, 2000; Kandlikar *et al*., 2005).

The presented scenarios of seasonal temperature and precipitation changes and the associated methodology give rise to further discussion and research. Other parameters, such as precipitation frequency and intensity could give more insight to the changes in the hydrological cycle. In principle, the study could be extended to other regions in the Alps or in Europe, notably to regions with different signal-to-noise ratios (noise referring here to model uncertainty and internal variability). This would allow for a differentiation between model uncertainty and internal decadal variability in the climate-change signals under different climatic conditions. Further work may aim towards extending the Bayesian algorithm such that internal decadal variability and uncertainties arising from RCM and GCM projections are included as additional terms to be explicitly modelled. That way, estimation uncertainties that are inherent here in the preprocessing part could be directly considered in the statistical model. From a user perspective, it would also be very helpful, that a new extended version of the algorithm will be capable of projecting climate change for several future scenario periods in the same model. These extensions could make the Bayesian algorithm of Buser *et al*. (2009) even more valuable for the climate change assessments at various spatial and temporal scales. As has been demonstrated in this study, the advantage in using such a Bayesian framework is not only that it provides probabilistically sound uncertainty estimates of climate change projections. The main advantage is that it rather forces the user to formulate and justify the assumptions to be made, so that it becomes clear what the probabilistic climate projections have been conditioned upon. This strongly increases the transparency of climate projections and facilitates their communication. Assumptions that are based on weak arguments can easily be identified.

Acknowledgements

We acknowledge the RCM datasets and E-OBS dataset from the EU-FP6 project ENSEMBLES (http://ensembles-eu.metoffice.com) and the data providers in the ECA & D project (http://eca.knmi.nl). This research was partly funded by the Swiss National Science Foundation through the National Centre for Competence in Research (NCCR) Climate, the Center for Climate Systems Modelling (C2SM) at ETH Zurich, and by the ENSEMBLES project (EU FP6, Contract GOCE-CT-2003-505539).

References

Allan RP, Soden BJ. 2007. Large discrepancy between observed and simulated precipitation trends in the ascending and descending branches of the tropical circulation. *Geophysical Research Letters* **34**: L18705, DOI: 10.1029/2007GL031460.

Begert M, Schlegel T, Kirchhofer W. 2005. Homogeneous temperature and precipitation series of Switzerland from 1864 to 2000. *International Journal of Climatology* **25**: 65–80, DOI: 10.1002/joc.1118.

Box GEP, Cox DR. 1964. An Analysis of Transformations. *Journal of the Royal Statistical Society* **26**: 211–252.

Buser CM, Künsch HR, Lüthi D, Wild M, Schär C. 2009. Bayesian multi-model projection of climate: bias assumptions and interannual variability. *Climate Dynamics* **33**: 849–868, DOI: 10.1007/s00382-009-0588-6.

Buser CM, Künsch HR, Schär C. 2010a. Bayesian multi-model projections of climate: generalization and application to ENSEMBLES results. *Climate Research* **44**: 227–241, DOI: 10.3354/cr00895.

Buser CM, Künsch HR, Weber A. 2010b. Biases and Uncertainty in Climate Projections. Scandinavian *Journal of Statistics* **37**: 179–199, DOI: 10.1111/j.1467–9469.2009.00686.x.

Ceppi P, Scherrer SC, Fischer AM, Appenzeller C. 2010. Revisiting Swiss temperature trends 1959–2008. *International Journal of Climatology* DOI: 10.1002/joc.2260.

CH2011. 2011. Swiss Climate Change Scenarios CH2011. Published by C2SM, MeteoSwiss, ETH, NCCR Climate, and OcCC. Zurich, Switzerland, ISBN: 978-3-033-03065-7.

Chatfield C. 2004. *The analysis of time series: an introduction*. 6th edition. Chapman and Hall: New York.

Christensen JH, Boberg F, Christensen OB, Lucas-Picher P. 2008. On the need for bias correction of regional climate change projections of temperature and precipitation. *Geophysical Research Letters* **35**(20): L20709, DOI: 10.1029/2008gl035694.

Christensen JH, Christensen OB. 2007. A summary of the PRUDENCE model projections of changes in European climate by the end of this century. *Climatic Change* **81**: 7–30, DOI: 10.1007/s10584-006-9210-7.

Cox P, Stephenson D. 2007. Climate change – A changing climate for prediction. *Science* **317**: 207–208, DOI: 10.1126/science.1145956.

Déqué M, Rowell DP, Lüthi D, Giorgi F, Christensen JH, Rockel B, Jacob D, Kjellström E, de Castro M, van den Hurk B. 2007. An intercomparison of regional climate simulations for Europe: assessing uncertainties in model projections. *Climatic Change* **81**: 53–70, DOI: 10.1007/s10584-006-9228-x.

Fischer EM, Schär C. 2009. Future Changes in daily summer temperature variability: driving processes and role for temperature extremes. *Climate Dynamics* **33**(7): 917–935, DOI: 10.1007/s00382-008-0473-8.

Fischer EM, Schär C. 2010. Consistent geographical patterns of changes in high-impact European heatwaves. *Nature Geoscience* **3**(6): 398–403, DOI: 10.1038/ngeo866.

Fischer EM, Seneviratne SI, Lüthi D, Schär C. 2007. Contribution of land-atmosphere coupling to recent European summer heat waves. *Geophysical Research Letters* **34**: L06707, DOI: 10.1029/2006GL029068.

Fowler HJ, Blenkinsop S, Tebaldi C. 2007. Linking climate change modelling to impacts studies: recent advances in downscaling techniques for hydrological modelling. *International Journal of Climatology* **27**(12): 1547–1578, DOI: 10.1002/joc.1556.

Frei C. 2004. *Die Klimazukunft der Schweiz – eine probabilistische Projektion*. (http://www.occc.ch/Products/CH2050/CH2050-Scenarien.pdf).

Furrer R, Knutti R, Sain SR, Nychka DW, Meehl GA. 2007. Spatial patterns of probabilistic temperature change projections from a multivariate Bayesian analysis. *Geophysical Research Letters* **34**: L06711, DOI: 10.1029/2006GL027754.

Gilks WR, Richardson S, Spiegelhalter DJ. 1996. *Markov Chain Monte Carlo in practice*. Chapman and Hall: London, UK.

Hawkins E, Sutton R. 2009. The potential to narrow uncertainty in regional climate predictions. *Bulletin of the American Meteorological Society* **90**(8): 1095–1107, DOI: 10.1175/2009bams2607.1.

Hawkins E, Sutton R. 2011. The potential to narrow uncertainty in projections of regional precipitation change. *Climate Dynamics* **37**:, DOI: 10.1007/s00382-010-0810-6.

Haylock MR, Hofstra N, Klein Tank AMG, Klok EJ, Jones PD, New M. 2008. A European daily high-resolution gridded data set of surface temperature and precipitation for 1950–2006. *Journal of Geophysical Research-Atmospheres* **113**: D20119, DOI: 10.1029/2008jd010201.

Hofstra N, New M, McSweeney C. 2010. The influence of interpolation and station network density on the distributions and trends of climate variables in gridded daily data. *Climate Dynamics* **35**: 841–858, DOI: 10.1007/s00382-009-0698-1.

Hohenegger C, Brockhaus P, Bretherton CS, Schär C. 2009. The Soil Moisture-Precipitation Feedback in Simulations with Explicit and Parameterized Convection. *Journal of Climate* **22**: 5003–5020, DOI: 10.1175/2009JCLI2604.1.

Hurrell, JW, van Loon H. 1997. Decadal variations in climate associated with the north Atlantic oscillation. *Climatic Change* **36**: 301–326, DOI: 10.1023/A:1005314315270.

IPCC. 2007. *Climate Change 2007: The Physical Science Basis. Contribution of Working Group I to the Fourth Assessment Report of the Intergovernmental Panel on Climate Change*. Solomon S, Qin D, Manning M, Chen Z, Marquis M, Averyt KB, Tignor M, Miller HL (eds). Cambridge University Press: Cambridge, UK.

Jacob D, Barring L, Christensen OB, Christensen JH, de Castro M, Déqué M, Giorgi F, Hagemann S, Lenderink G, Rockel B, Sanchez E, Schär C, Seneviratne SI, Somot S, van Ulden A, van den Hurk B. 2007. An inter-comparison of regional climate models for Europe: model performance in present-day climate. *Climatic Change* **81**: 31–52, DOI: 10.1007/s10584-006-9213-4.

Jenkins GJ, Murphy JM, Sexton DS, Lowe JA, Jones P, Kilsby CG. 2009. *UK Climate Projections. Briefing Report*. Met Office Hadley Centre: Exeter, UK. (http://ukclimateprojections.defra.gov.uk).

Jun M, Knutti R, Nychka DW. 2008. Spatial Analysis to Quantify Numerical Model Bias and Dependence: How Many Climate Models Are There? *Journal of the American Statistical Association* **103**(483): 934–947, DOI: 10.1198/016214507000001265.

Kandlikar M, Risbey J, Dessai S. 2005. Representing and communicating deep uncertainty in climate-change assessments. *Comptes Rendus Geoscience* **337**: 443–455, DOI: 10.1016/j.crte.2004.10.010.

Kjellström E, Nikulin G, Hansson U, Strandberg G, Ullerstig A. 2010. 21st century changes in the European climate: uncertainties derived from an ensemble of regional climate model simulations. *Tellus A* **63**: 24–40, DOI: 10.1111/j.1600-0870.2010.00475.x.

Klein Tank AMG, Lenderink G. 2009. *Climate Change in the Netherlands: Supplement to the KNMI'06 Scenarios*. KNMI: De Bilt, The Netherlands.

Knutti R, Allen MR, Friedlingstein P, Gregory JM, Hegerl GC, Meehl GA, Meinshausen M, Murphy JM, Plattner GK, Raper SCB, Stocker TF, Stott PA, Teng H, Wigley TML. 2008. A review of uncertainties in global temperature projections over the twenty-first century. *Journal of Climate* **21**: 2651–2663, DOI: 10.1175/2007JCLI2119.1.

Knutti R, Furrer R, Tebaldi C, Cermak J, Meehl GA. 2010. Challenges in Combining Projections from Multiple Climate Models. *Journal of Climate* **23**(10): 2739–2758, DOI: 10.1175/2009jcli3361.1.

Knutti R, Hegerl GC. 2008. The equilibrium sensitivity of the Earth's temperature to radiation changes. *Nature Geoscience* **1**(11): 735–743, DOI: 10.1038/ngeo337.

Kysely J, Plavcova E. 2010. A critical remark on the applicability of E-OBS European gridded temperature data set for validating control climate simulations. *Journal of Geophysical Research-Atmospheres* **115**: D23118, DOI: 10.1029/2010JD014123.

Lempert RJ, Schlesinger ME. 2000. Robust strategies for abating climate change – An editorial essay. *Climatic Change* **45**(3): 387–401, DOI: 10.1023/A:1005698407365.

Lenderink G, van Ulden A, van den Hurk B, Keller F. 2007. A study on combining global and regional climate model results for generating climate scenarios of temperature and precipitation for the Netherlands. *Climate Dynamics* **29**(2): 157–176, DOI: 10.1007/s00382-007-0227-z.

Masson D, Knutti R. 2011. Climate Model Genealogy. *Geophysical Research Letters* **38**: L08703, DOI: 10.1029/2011GL046864.

Mearns LO. 2010. The drama of uncertainty. *Climatic Change* **100**(1): 77–85, DOI: 10.1007/s10584-010-9841-6.

Meinshausen M, Meinshausen N, Hare W, Raper SCB, Frieler K, Knutti R, Frame DJ, Allen MR. 2009. Greenhouse-gas emission targets for limiting global warming to 2 degrees C. *Nature* **458**(7242): 1158–1162, DOI: 10.1038/nature08017.

Mitchell, TD 2003. Pattern scaling – An examination of the accuracy of the technique for describing future climates. *Climatic Change* **60**(3): 217–242, DOI: 10.1023/A:1026035305597.

Murphy JM, Booth BBB, Collins M, Harris GR, Sexton DMH, Webb MJ. 2007. A methodology for probabilistic predictions of regional climate change from perturbed physics ensembles. *Philosophical Transactions of the Royal Society a-Mathematical Physical and Engineering Sciences* **365**(1857): 1993–2028, DOI: 10.1098/rsta.2007.2077.

Murphy JM, Sexton DMH, Barnett DN, Jones GS, Webb MJ, Collins M. 2004. Quantification of modelling uncertainties in a large ensemble of climate change simulations. *Nature* **430**: 768–772, DOI: 10.1038/nature02771.

Nakicenovic N, Swart R. 2000. *IPCC Special Report on Emissions Scenarios*. Cambridge University Press: Cambridge, UK.

OcCC. 2007. *Climate change and Switzerland 2050. Expected Impacts on Environment, Society and Economy*. OcCC/ProClim: Berne, Switzerland.

Räisänen J. 2007. How reliable are climate models? *Tellus Series a-Dynamic Meteorology and Oceanography* **59**(1): 2–29, DOI: 10.1111/j.1600-0870.2006.00211.x.

Rowell DP, Jones RG. 2006. Causes and uncertainty of future summer drying over Europe. *Climate Dynamics* **27**: 281–299, DOI: 10.1007/s00382-006-0125-9.

Santer BD, Wigley TML, Schlesinger ME, Mitchell JFB. 1990. *Developing Climate Scenarios from Equilibrium GCM results.* MPI Report 47: Hamburg, Germany. (http://www.mpimet.mpg.de/fileadmin/publikationen/Reports/Report_47.pdf).

Scherrer SC, Appenzeller C, Liniger MA, Schär C. 2005. European temperature distribution changes in observations and climate change scenarios. *Geophysical Research Letters* **32**: L19705, DOI: 10.1029/2005GL024108.

Schär C, Vidale PL, Lüthi D, Frei C, Häberli C, Liniger MA, Appenzeller C. 2004. The role of increasing temperature variability in European summer heatwaves. *Nature* **427**(6972): 332–336, DOI: 10.1038/nature02300.

Seneviratne SI, Lüthi D, Litschi M, Schär C. 2006. Land-atmosphere coupling and climate change in Europe. *Nature* **443**(7108): 205–209, DOI: 10.1038/nature05095.

Stott PA, Tett SFB, Jones GS, Allen MR, Mitchell JFB, Jenkins GJ. 2000. External Control of 20th Century Temperature by Natural and Anthropogenic Forcings. *Science* **290**(5499): 2133–2137, DOI: 10.1126/science.290.5499.2133.

Tebaldi C, Knutti R. 2007. The use of the multi-model ensemble in probabilistic climate projections. *Philosophical Transactions of the Royal Society a-Mathematical Physical and Engineering Sciences* **365**(1857): 2053–2075, DOI: 10.1098/rsta.2007.2076.

Tebaldi C, Smith RL, Nychka D, Mearns LO. 2005. Quantifying uncertainty in projections of regional climate change: A Bayesian approach to the analysis of multimodel ensembles. *Journal of Climate* **18**(10): 1524–1540, DOI: 10.1175/JCLI3363.1.

van der Linden P, Mitchell JFB. 2009. *ENSEMBLES: Climate change and its Impacts: Summary of research and results from the ENSEMBLES project.* Met Office Hadley Centre: Exeter, UK.

van Oldenborgh GJ, Drijfhout S, van Ulden AP, Haarsma R, Sterl A, Severijns C, Hazeleger W, Dijkstra H. 2009. Western Europe is warming much faster than expected. *Climate of the Past* **5**: 1–12.

van Ulden AP, van Oldenborgh GJ. 2006. Large-scale atmospheric circulation biases and changes in global climate model simulations and their importance for climate change in Central Europe. *Atmospheric Chemistry and Physics* **6**: 863–881.

van Vuuren DP, Den Elzen MGJ, Lucas PL, Eickhout B, Strengers BJ, van Ruijven B, Wonink S, van Houdt R. 2007. Stabilizing greenhouse gas concentrations at low levels: an assessment of reduction strategies and costs. *Climatic Change* **81**(2): 119–159, DOI: 10.1007/s10584-006-9172-9.

Vidale PL, Lüthi D, Wegmann R, Schär C. 2007. European summer climate variability in a heterogeneous multi-model ensemble. *Climatic Change* **81**: 209–232, DOI: 10.1007/s10584-006-9218-z.

Weigel AP, Knutti R, Liniger MA, Appenzeller C. 2010. Risks of Model Weighting in Multimodel Climate Projections. *Journal of Climate* **23**(15): 4175–4191, DOI: 10.1175/2010jcli3594.1.

Weigel AP, Liniger MA, Appenzeller C. 2008. Can multi-model combination really enhance the prediction skill of probabilistic ensemble forecasts? *Quarterly Journal of the Royal Meteorological Society* **134**(630): 241–260, DOI: 10.1002/qj.210.

Wu PL, Wood R, Ridley J, Lowe J. 2010. Temporary acceleration of the hydrological cycle in response to a CO2 rampdown. *Geophysical Research Letters* **37**: L12705, DOI: 10.1029/2010GL043730.

Zhang XB, Zwiers FW, Hegerl GC, Lambert FH, Gillett NP, Solomon S, Stott PA, Nozawa T. 2007. Detection of human influence on twentieth-century precipitation trends. *Nature* **448**: 461–465, DOI: 10.1038/nature06025.

